European Journal of Medicinal Chemistry 266 (2024) 116128

Contents lists available at ScienceDirect

European Journal of Medicinal Chemistry

journal homepage: www.elsevier.com/locate/ejmech

Research paper

Peptidomimetics as potent dual SARS-CoV-2 cathepsin-L and main protease inhibitors: In silico design, synthesis and pharmacological characterization

Tania Ciaglia [a], Vincenzo Vestuto [a], Veronica Di Sarno [a], Simona Musella [a], Gerardina Smaldone [a], Francesca Di Matteo [a], Valeria Napolitano [a], Maria Rosaria Miranda [a], Giacomo Pepe [a], Manuela Giovanna Basilicata [a], Sara Novi [a], Ilaria Capolupo [a], Giuseppe Bifulco [a], Pietro Campiglia [a,b], Isabel Gomez-Monterrey [c], Robert Snoeck [d], Graciela Andrei [d], Michele Manfra [e], Carmine Ostacolo [a], Gianluigi Lauro [a,*], Alessia Bertamino [a,**]

[a] Department of Pharmacy, University of Salerno, Via G. Paolo II 132, 84084, Fisciano, Salerno, Italy
[b] European Biomedical Research Institute (EBRIS), Via S. De Renzi 50, 84125, Salerno, Italy
[c] Department of Pharmacy, University Federico II of Naples, Via D. Montesano 49, 80131, Naples, Italy
[d] Rega Institute for Medical Research, Department of Microbiology, Immunology, and Transplantation, KU Leuven, BE-3000, Leuven, Belgium
[e] Department of Science, University of Basilicata, Via Dell'Ateneo Lucano 10, 85100, Potenza, Italy

ARTICLE INFO

Keywords:
Pepetidomimetcs
SARS-CoV-2 cathepsin-L and main protease inhibition
Antiviral drugs
In silico design
In-cell assays

ABSTRACT

In this paper we present the design, synthesis, and biological evaluation of a new series of peptidomimetics acting as potent *anti*-SARS-CoV-2 agents. Starting from our previously described Main Protease (M^{Pro}) and Papain Like Protease (PL^{Pro}) dual inhibitor, **CV11**, here we disclose its high inhibitory activity against cathepsin L (CTSL) ($IC_{50} = 19.80 \pm 4.44$ nM), an emerging target in SARS-CoV-2 infection machinery. An *in silico* design, inspired by the structure of **CV11**, led to the development of a library of peptidomimetics showing interesting activities against CTSL and M^{pro}, allowing us to trace the chemical requirements for the binding to both enzymes. The screening in Vero cells infected with 5 different SARS-CoV-2 variants of concerns, highlighted sub-micromolar activities for most of the synthesized compounds (**13**, **15**, **16**, **17** and **31**) in agreement with the enzymatic inhibition assays results. The compounds showed lack of activity against several different RNA viruses except for the 229E and OC43 human coronavirus strains, also characterized by a cathepsin-L dependent release into the host cells. The most promising derivatives were also evaluated for their chemical and metabolic *in-vitro* stability, with derivatives **15** and **17** showing a suitable profile for further preclinical characterization.

1. Introduction

The coronavirus disease 2019 (COVID-19) pandemic, triggered by the severe acute respiratory syndrome coronavirus 2 (SARS-CoV-2) is considered among the most tremendous health catastrophe in the last centuries, causing 771 million of contagious and almost 7 million of deaths worldwide [1]. Despite all the efforts made in social, economic and health fields since its outbreak in 2019, after four years we are not still able to eradicate this plague.

SARS-CoV-2 is a positive-sense single-stranded RNA, enveloped virus, belonging to the *betacoronavirus* genus, family Coronaviridae, and its peculiarity is represented by the envelope protein, Spike (SP), which gives it a typical crown shape. SP is responsible for the virus entry in the host cells through the cellular angiotensin converting enzyme receptor 2 (ACE2R) recognition [2].

SARS-CoV-2 infection is principally related to airways impairment [3], and it is possible to schematize the disease in 3 different stages: 1) active virus replication in the host cells, with benign symptoms very similar to other sicknesses, such as colds and flu; 2) lung function compromission, frequently accompanied by bilateral pneumonia with serious respiratory symptomatology; 3) cytokines storm, characterized by hyperinflammation which can lead to morphological lung alteration,

* Corresponding author.
** Corresponding author.
E-mail addresses: glauro@unisa.it (G. Lauro), abertamino@unisa.it (A. Bertamino).

https://doi.org/10.1016/j.ejmech.2024.116128
Received 6 November 2023; Received in revised form 11 December 2023; Accepted 4 January 2024
Available online 9 January 2024

vasculopathy and thrombosis [4].

From the therapeutic point of view, in the two initial phases of the illness, the objective is reducing the viral replication, while decreasing the host hyperinflammatory response to contain its consequences in the third step. For this reason, the *anti*-SARS-CoV-2 therapeutics can be classified in two categories, depending on their ability in reducing the host immune response, or in decreasing the virus replication. These latter are further divided into agents inhibiting RNA duplication and transcription and agents disrupting the SP/ACE2R binding [5].

In the last few years, several drugs have been approved for the treatment of the most severe cases. However, the vaccine campaign has represented the outstanding strategy to contain the contagious wave. Among all therapeutic options, antiviral drugs are considered a milestone of the pharmacological intervention, but very few medicaments are currently available [6]: remdesivir as RNA polymerase (RNAp) inhibitor [7], nirmatrelvir–ritonavir association inhibiting the viral main protease (MPro) [8] and molnupiravir as inhibitor of SARS-CoV-2 replication [9]. Together with these antiviral drugs, monoclonal antibodies (mAbs) have been developed to treat SARS-CoV-2 infection. The mAbs can act either by inhibiting the virus entry and targeting viral machinery, promoting its elimination, or by neutralizing cytokines storm [10]. Only seven *anti*-SARS-CoV-2 mAbs, namely bamlanivimab, etesevimab, casirivimab, imdevimab, sotrovimab, cilgavimab and tixagevimab have been approved so far [11]. This kind of therapy is useful for the most severe infections, but many cases of loss of efficacy have been reported in the most recent period, due to the latest emerging SARS-CoV-2 variants [12]. Indeed, the activity of *anti*-SARS-CoV mAbs can vary significantly against specific variants and subvariants (PMID: 37876803; PMID: 35857646).

RNA viruses, normally, have high mutation rates allowing them an extreme capacity for rapid evolution, because of their low-fidelity RNA polymerases. Among these, SARS-CoV-2, as coronaviruses family member, is subjected to a minor rate of mutations, thanks to its proofreading machinery capable of excising mis-incorporated nucleotides from the growing RNA [13–15]. Nevertheless, since the end of 2019, when the outbreak of COVID-19 pandemic became, a significative number of variants emerged. In November 2021, the WHO proclaimed the new omicron variant, known as B.1.1.529, as variant of concern (VOC) and until now, numerous omicron subvariants have been identified [16,17]. The most common mutations (34 missense mutations) in omicron subtypes, occur in Spike Protein, principally located at the receptor-binding domain (RBD) (15 mutations) [18,19] penalizing the drugs acting by SP modulation [20], and vaccines [21], which needed to be rapidly updated [22,23].

It is clear that, even if the most dangerous wave of contagious SARS-CoV-2 should have been overcome, the necessity to expand the therapeutic arsenal against SARS-CoV-2 to protect us from the estimated very long permanence of the virus is still very urgent. In this context, SARS-CoV-2 proteases, Main Protease (M^{Pro}) and Papain Like Protease (PL^{Pro}), because of their crucial role in the viral replication machinery, have inspired the pharmaceutical research to develop new inhibitors for tackling the virus [24–28]. Recently, another protease, namely Cathepsin-L (CTSL), has elicited much appeal because of its involvement in the initial stage of the virus infection. CTSL is a lysosome cysteine protease that comes into play when the virus is endocytosed by the host cell, cleaving the Spike Protein and, in this way, activating its fusion potential [29]. Recently, it has been demonstrated that CTSL levels are increased in COVID-19 patients and that they can be related to the different stages of the pathology [30]. This evidence paved the way for an extended investigation about this new pharmacological target, triggering the discovery of CTSL inhibitors useful in the fight against SARS-CoV-2 [31–33].

Surprisingly, a great input to the discovery of CTSL inhibitors came by serendipity, during M^{Pro} inhibitors discovery studies, since the two targets share a high level of homology [34–36].

Starting from these premises and from our previous results in the identification of new SARS-CoV-2 proteases inhibitors [37], we wondered if our lead compound, **CV11** (Fig. 1), could be also suitable as CTSL blocker and, indeed, we disclosed a very high CTSL inhibitory activity (Table 1). This result inspired the design and the synthesis of a new series of peptidomimetics deriving from the structure of compound **CV11**, by variating the tryptophan residue, the butylene side chain, the chloroacetyl substituent and the benzyl moiety (Fig. 1). The obtained derivatives were characterized by a remarkable CTSL enzymatic inhibition often associated to a synergic M^{pro} activity interference, and high antiviral potency. Moreover, these compounds also showed promising *in-vitro* pharmacokinetic properties, paving the way for further pre-clinical characterization.

2. Results and discussion

2.1. Chemistry

Final pseudo-peptides **13**–**20**, **22** and **25** were synthesized according to Scheme 1.

Boc-L-Tryptophane was treated with benzylamine in classic coupling conditions, using HOBt, HBTU and DIPEA in DCM leading to intermediate **1** in 80 % yield. After Boc protecting group removal with TFA in DCM (1/3 as ratio) and using TIS as scavenger, the α-amino group of compound **2** was coupled with Boc-L-Leu-OH, or Boc-D-Leu-OH, or Boc-L-Phe-OH or Boc-Gly-OH, or Boc-L-Tyr-OH in the same conditions discussed above. Pseudo-dipeptides **3**–**7** were obtained in a range of 65–82 % of yields. Amino group deprotection of intermediates **3**–**7** in the same conditions described before, almost quantitatively, led to derivatives **8**–**12** that were treated with the proper acyl chloride to furnish final compounds **13**–**20** (48–68 % yields).

Intermediate **10** was also coupled with Boc-L-Leu-OH in the previous described conditions, giving, after Boc removal, compound **21** (78 % yield), which was reacted with chloroacetyl chloride in DCM using TEA as base, yielding final derivative **22** in 52 % yield.

Starting from Boc-D-Trp-OH, following the same pathway and the same reaction conditions described for the synthesis of **13**, final compound **25** was obtained in 36 % of overall yield.

Compounds **28**, **31** and **33** were obtained as depicted in Scheme 2.

Using Boc-L-Trp-OH as starting material, coupling reaction with 4-(2-aminoethyl)morpholine employing HOBt and HBTU as coupling agents and DIPEA as base, compound **26** was obtained in 74 % yield. A cycle of Boc deprotection in DCM/TFA (3/1 as ratio) in presence of TIS, and a further coupling with Boc-L-Allyl-Gly-OH in the same reaction conditions described above, afforded intermediate **27** (58 % yield).

Compound **28** was obtained in 52 % yield, after a classical Boc removal and subsequent reaction with chloroacetyl chloride in DCM and TEA.

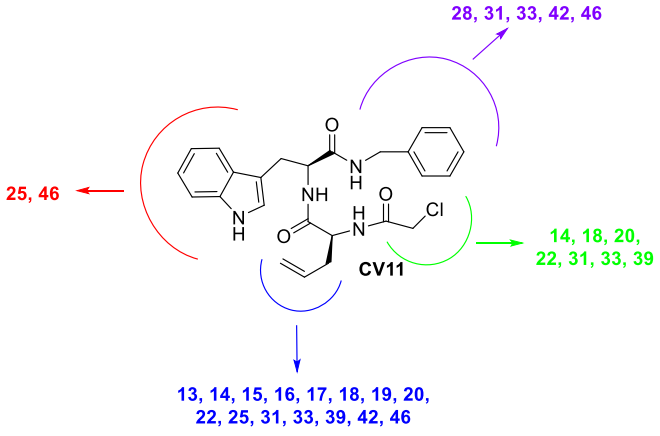

Fig. 1. Design of peptidomimetics starting from the structure of **CV11**.

Table 1
Measured Activities for inhibition of SARS-CoV-2 selected protein targets.

Compound	Structure	M^{pro}	CTSL
		IC_{50} (nM)	IC_{50} (nM)
GC-376		570.23 ± 23.12	–
E-64		–	34.01 ± 8.70
CV11	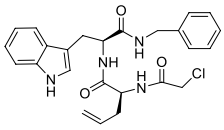	1720.44 ± 440.66	19.80 ± 4.44
13	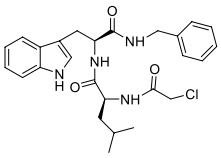	2810.81 ± 520.18	2.82 ± 0.76
14	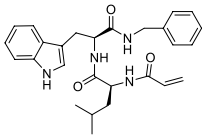	>30000	26040.17 ± 1120.00
15	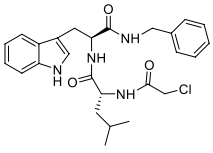	>30000	100.54 ± 21.46
16	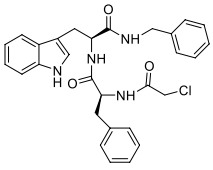	730.12 ± 320.37	3.17 ± 0.87
17	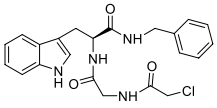	>30000	32.50 ± 19.57
18	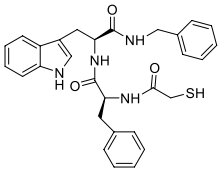	>30000	5080.47 ± 2180.03
19	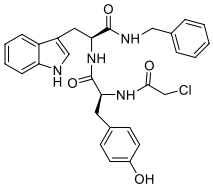	8350.53 ± 1850.32	50.25 ± 23.25

(*continued on next page*)

Table 1 (*continued*)

Compound	Structure	M^{pro}	CTSL
		IC_{50} (nM)	IC_{50} (nM)
20	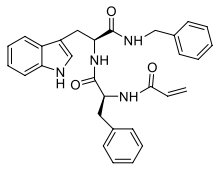	>30000	>30000
22	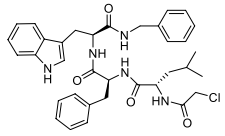	>30000	8.01 ± 2.12
25	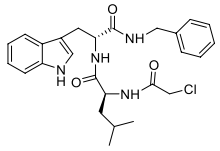	14610.54 ± 2120.47	2920.33 ± 790.30
28	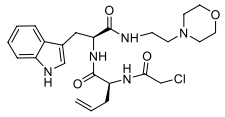	>30000	206.78 ± 98.10
31	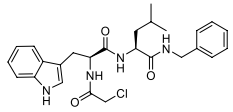	8320.26 ± 890.36	10.30 ± 5.64
33	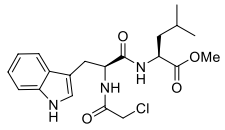	>30000	27410.78 ± 3150.27
39	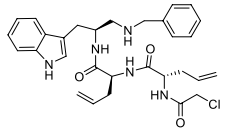	>30000	314.41 ± 121.07
42	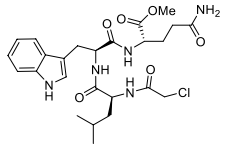	>30000	82.93 ± 22.67
46	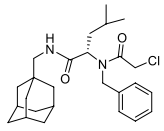	>30000	3020.15 ± 1560.53

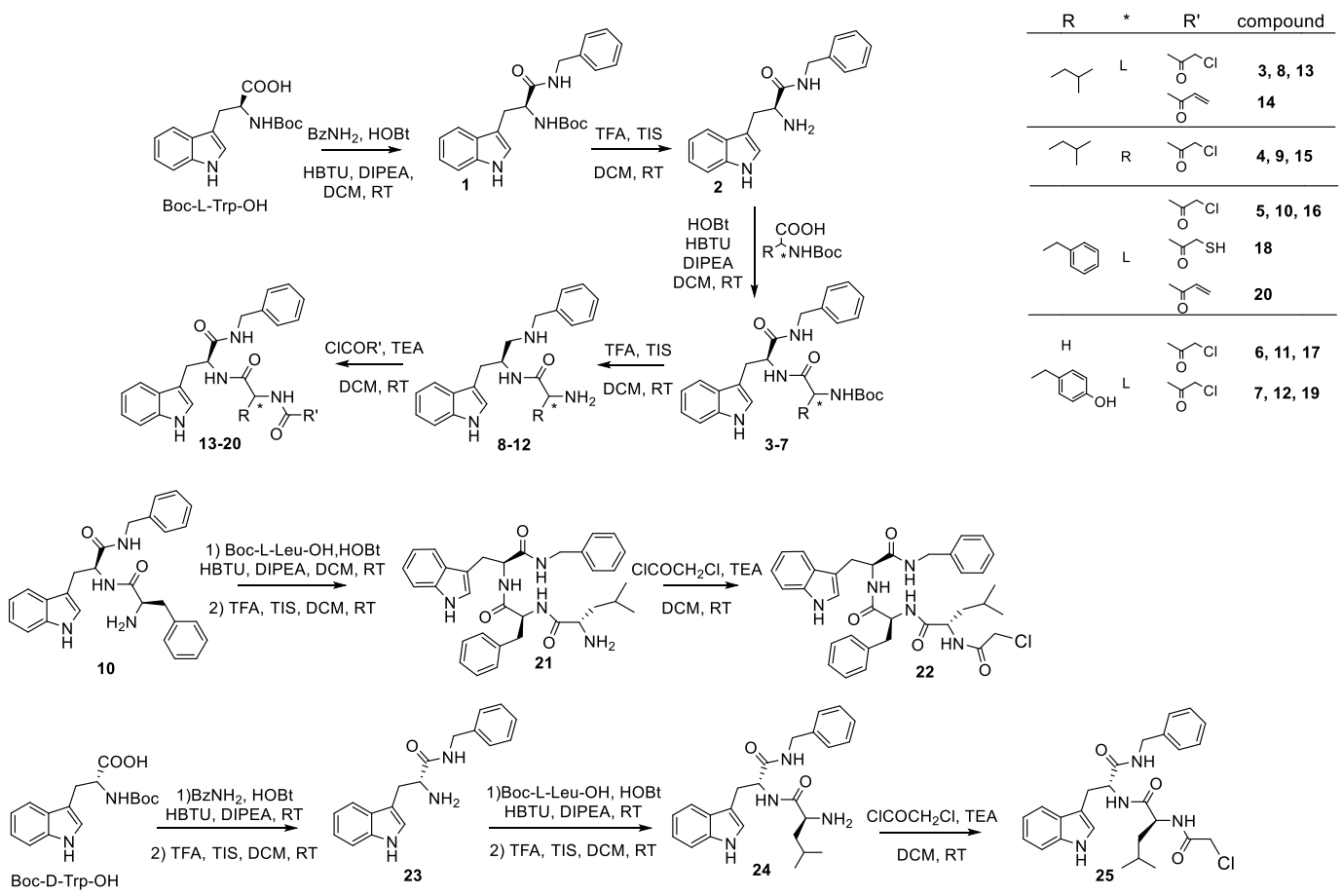

Scheme 1. Synthesis of compounds **13**–**20**, **22** and **25**.

Derivative **31** was synthesized starting from Boc-L-Trp-OH, that was coupled with L-Leu-OMe, using the previously described reaction conditions to yield intermediate **29**. Hydrolysis of methyl ester in aqueous NaOH and subsequent coupling with benzylamine, employing HOBt, HBTU and DIPEA afforded **30**. The last reaction steps consisted in Boc removal and acyl substitution with chloroacetyl chloride leading to final compound **31** in 21 % overall yield.

Starting from methyl (*tert*-butoxycarbonyl)-L-tryptophyl-L-leucinate (**29**), deprotection with TFA/DCM (1:3 v:v) and TIS led to **32**, that was subsequently treated with chloroacetyl chloride in DCM and TEA, affording final compound **33** in 45 % of overall yield.

Compounds **39**, **42** and **46** were obtained in accordance with Scheme 3.

Commercially available Cbz-L-Trp-OH was subjected to Weinreb amidation with N,O-dimethyl hydroxylamine, HOBt, HBTU and DIPEA, to furnish the carbamoyl intermediate **34**, in 85 % yield. Weinreb amide was reduced to the corresponding aldehyde using $LiAlH_4$ and then, subjected to reductive amination with benzylamine, affording compound **35** in 52 % yield. The introduction of Boc protecting group using Boc anhydride in DCM, and Cbz removal under hydrogenation conditions gave **36** in 88 % yield. Intermediate **36** was coupled with Fmoc-L-allyl-Gly-OH using HOBt, HBTU and DIPEA in DCM and then subjected to Fmoc removal in a mixture of diethylamine/DCM (1:3 v:v) leading to compound **37** (78 % yield). Another cycle of coupling and Fmoc-deprotection, using the same reagents and conditions just described, afforded pseudo tripeptide **38** in 72 % yield. Finally, compound **39** was obtained in 78 % yield by free amino-group reaction with chloroacetyl chloride and TEA in DCM and subsequent Boc deprotection in TFA/DCM (1:3 v:v) using TIS as scavenger.

Coupling reaction between Cbz-L-Trp-OH and L-Gln(Trt)-OMe using HOBt, HBTU and DIPEA generated dipeptide **40** (72 % yield), that was deprotected from Cbz group under reduction conditions and coupled with Fmoc-L-Leu-OH as described above to afford compound **41** in 68 % yield. After Fmoc removal in DEA/DCM (1:3 v:v), NH_2 acylation with chloroacetyl chloride and, in the end, Boc deprotection in a mixture of TFA/DCM (1:3 v:v), final derivative **42** was obtained in 38 % yield.

Compound **46** was obtained starting from L-Leu-OMe, that was treated with benzaldehyde to form the corresponding immine derivative, that was reduced with $NaBH_4$ leading to compound **43** in 72 % yield. Boc protecting group was introduced on the secondary amine, using Boc anhydride and TEA in DCM, then the methyl ester function was hydrolized by aqueous NaOH to furnish intermediate **44** (38 % yield). Coupling reaction with 1-adamantanemethylamine in the same usual conditions gave intermediate **45** in 68 % yield; Boc removal in standard conditions and NH-acylation with chloroacetyl chloride, finally led to compound **46** in 38 % yield.

2.2. *In silico design and enzymatic inhibition results*

Our efforts in identifying novel agents able to interfere with SARS-CoV-2 virus were focused on the possibility of inhibiting CTSL protease supported by the recently disclosed key role of this protein in promoting and sustaining COVID-19 pathology [29–31]. The starting point of this study concerned the re-evaluation of our previously discovered **CV11** M^{pro} inhibitor as a new putative modulator of CTSL activity. Similar to the previous hypothesis for M^{pro} binding, molecular docking experiments were performed starting from the covalent binding between the Cys25 residue at the CTSL enzyme binding site, widely reported as the reactive nucleophile targeting electrophilic warheads [38,39] which is in this case the reactive chloroacetyl moiety of **CV11**. As widely

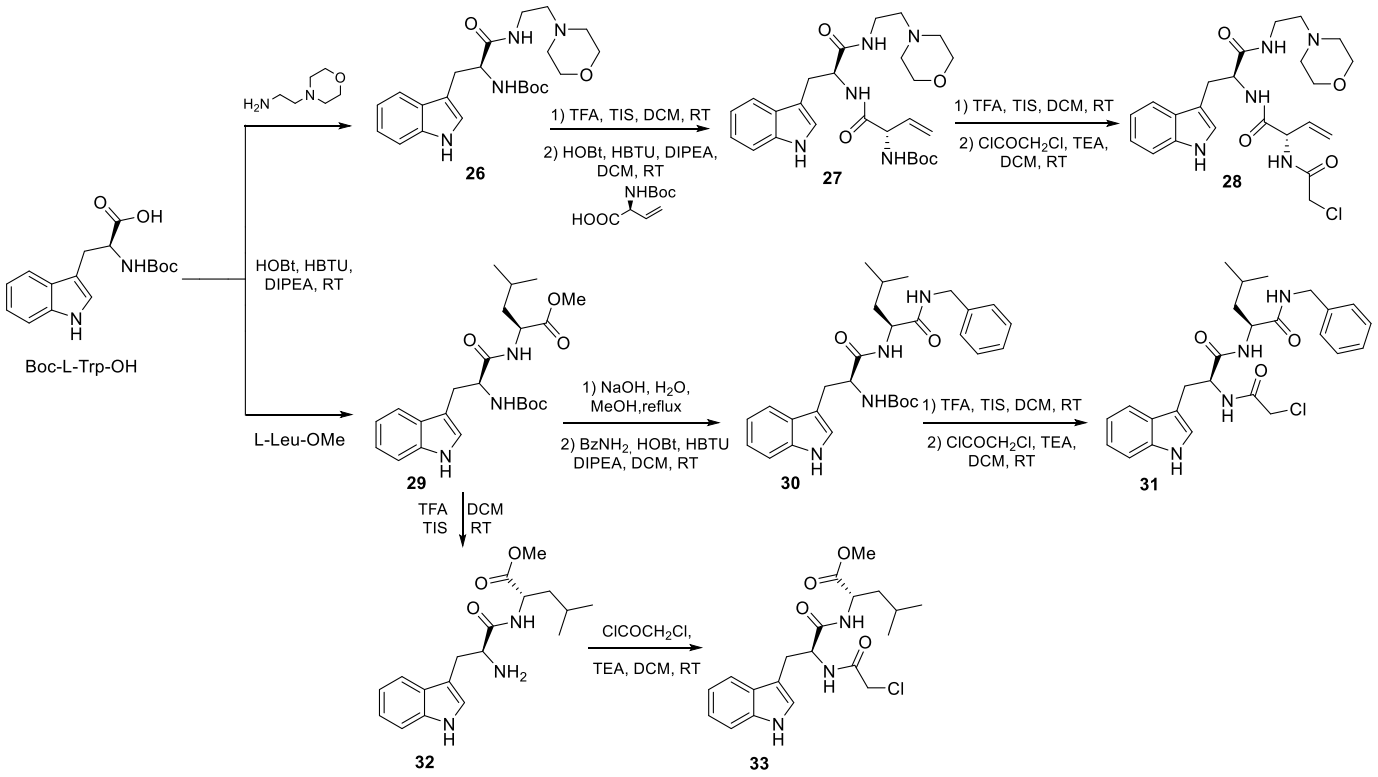

Scheme 2. Synthesis of compounds **28**, **31** and **33**.

reported, CTSL protein features six subsites (S1, S2, S3, S1′, S2′, S3', Cys25 reactive residue located at the S1 subsite) (Fig. 2A) that can be conveniently occupied by different types of binders [40]. Therefore, we carefully analysed the predicted binding poses of **CV11** according to these structural data.

In details, **CV11** is able to establish a large set of polar, hydrophobic, and π-π interactions with residues belonging to S1, S1′, and partly S3/S2' subsites. Both the indole and benzyl moieties make π-π contacts with His163 and Trp189, while the indole nitrogen interacts with the backbone of Ala138 through an H-bond. Further hydrogen bonds were detected with Gly18 and His163 (Fig. 2B). From this analysis, we then speculated that the aromatic moieties and, in particular, the indole was fundamental for CTSL binding since its ability to interact with Ala138, His163, Trp189 via π-π interactions, van der Waals contacts, and H-bond (Fig. 2B). Furthermore, we observed a partial occupation of the S3 subsite by the butenyl moiety of **CV11**, thus suggesting that this chemical portion should be carefully investigated to obtain analogues with enhanced potency (*vide infra*).

The computational hypothesis has been validated by an enzymatic assay in which **CV11** showed an interesting inhibitory potency with an IC_{50} of 19.80 ± 4.44 nM, higher than E−64 used as reference inhibitor [41].

Once assessed the importance of the indole group, to further validate the obtained outcomes from molecular docking experiments and to trace a structure-activity relationship (SAR), we first wondered whether the substitution of the benzyl moiety as the additional putative key aromatic group of **CV11** with a polar, non-aromatic group could affect the biological activity against CTSL. As expected, *in silico* data related to compound **28**, in which a 4-ethylmorpholine moiety was introduced, disclosed the lack of the π-π interaction with Trp189 (Fig. 3A) and biological results highlighted ten times higher IC_{50} detected for **28** if compared to **CV11** (Table 1). These combined *in silico*/biological data confirmed the importance of the benzyl moiety in binding the target protein. We then investigated whether variation in the position of the chloroacetyl group could affect the inhibitory activity. In particular, in the pseudo-tripeptide compound **39**, the introduction of an additional amino acid led to a binding mode not in line to that of **CV11** with different positions of the key benzyl and indole moieties in the binding site (Fig. 3B). Specifically, various interactions previously detected for **CV11** were no longer observed due to the different accommodation in the CTSL binding site and, specifically, **39** lacked π-π contacts with His163 and H-bond with Ala138 due to the different accommodation of the indole moiety within the S2' subsite, enhancing the IC_{50} of **39** about 16 times with respect to **CV11**.

The next step concerned the investigation of the role of the butenyl moiety in **CV11**, placed in the S3 subsite according to docking results (*vide supra*, Fig. 2). With this aim, this group was first removed (compound **17**) to assess its impact on modulating the inhibitory activity against CTSL and to further corroborate the predicted binding modes for the above reported investigated compounds. Docking results revealed a similar accommodation for **17** in the binding site if compared to **CV11** but, as expected, interactions with residues belonging to S3 subsite partially observed for **CV11** were here not observed (Fig. 3C). Biological outcomes were in line with *in silico* data and a slight decrease in inhibitory activity was detected (Table 1).

Accordingly, we replaced the butenyl group of **CV11** with a bulky isobutyl moiety (compound **13**) that occupied the S3 subsite in a satisfactory way due to the large volume of the new introduced chemical function. Biological data disclosed a remarkable improvement in the inhibitory activity against CTSL (IC_{50} = 2.82 ± 0.76 *vs* 19.80 ± 4.44 nM), thus highlighting the importance of this chemical moiety as predicted by docking experiments (Fig. 3D and Table 1). Starting from these data, we then synthesized a set of close derivatives to assess how punctual modifications could influence the biological activity. Similarly to what was already done for **CV11** and **28**, we proceeded with further investigations first replacing the benzyl group of **13** with a long, polar chain comprising both an ester and an amide function (compound **42**). Docking results further confirmed that the removal of the aromatic moiety caused the loss of the π-π interaction with Trp189 towards the S1′ subsite (Fig. 3E), and *in-vitro* data pointed out the reduction of the

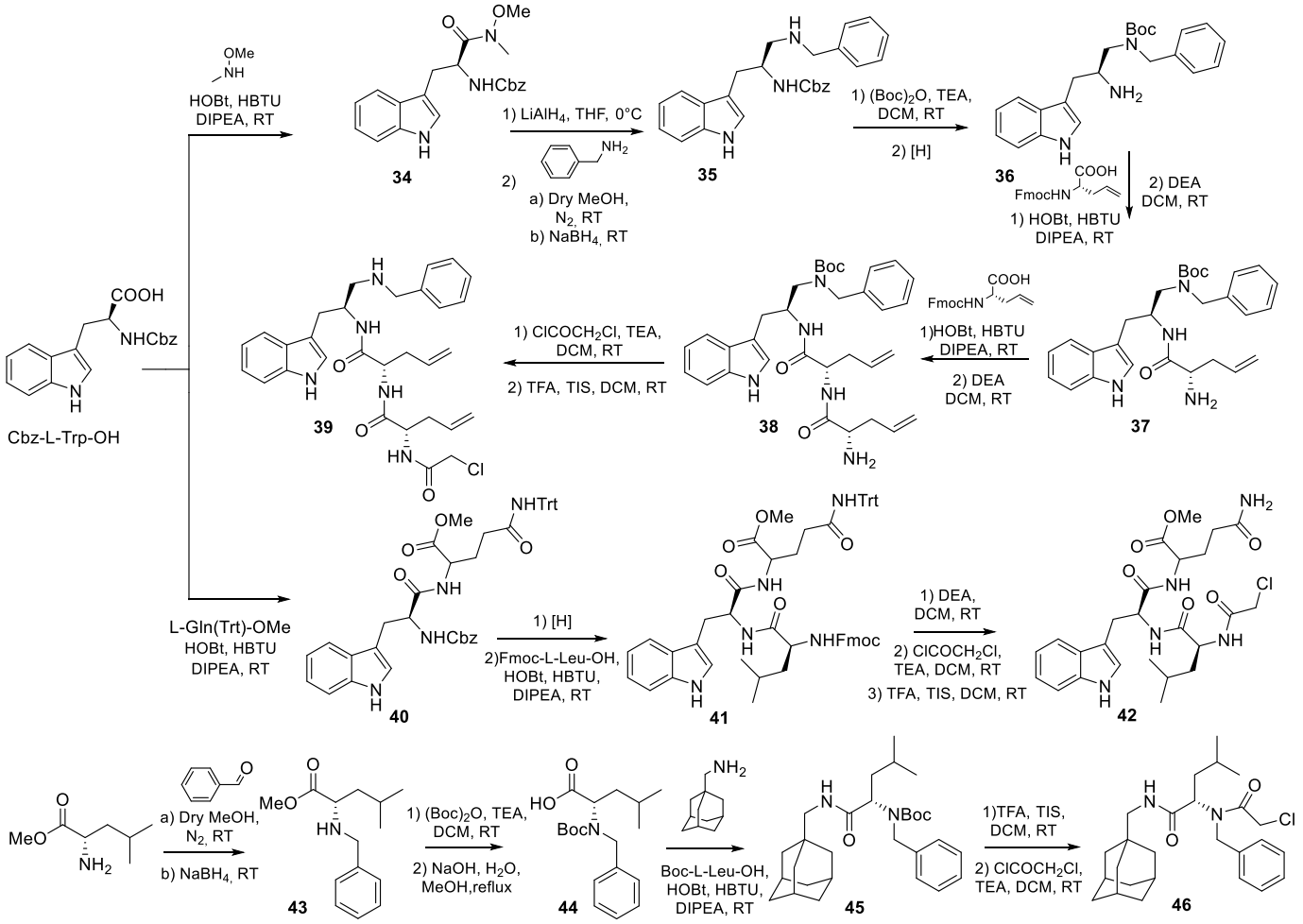

Scheme 3. Synthesis of compounds **39**, **42** and **46**.

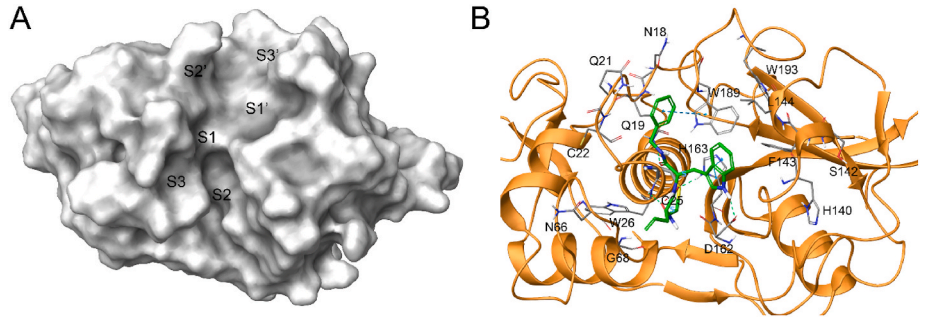

Fig. 2. A) Binding subsites of cathepsin L (CTSL) enzyme and their orientation on the protein structure (PDB code: 2XU3). Molecular surface of CTSL is depicted in light grey. B) **CV11** (colored by atom type: C green, O red, N blue, polar H light grey) in docking with CTSL (secondary structure in ribbons and colored in orange; key residues are reported as sticks and colored by atom type: C grey, O red, N blue, S yellow, polar H light grey). H-bonds and π-π interactions are reported in green and cyan dotted lines, respectively.

inhibitory activity for **42** if compared to **13** of about 30 times (Table 1). Furthermore, the modification of the position of the isobutyl moiety (compound **33**) caused a strong decrease of the CTSL inhibition resulting an IC_{50} in high micromolar range (Table 1), in accordance with computational data showing the lack of the π-π interaction with Trp189 belonging to S1' subsite and the non-occupancy of the S3 subsite (Fig. 3F). On the other hand, compound **31**, featuring both the isobutyl and benzyl moiety but differently placed on the pseudopeptidic skeleton if compared to **13**, featured a loss in inhibitory activity, even if it maintained a very good potency (10.30 ± 5.64 *vs* 2.82 ± 0.764 nM, Table 1). Indeed, a large set of hydrophobic contacts were detected and, above all, aromatic and van del Waals contacts were re-established between both the indole and benzyl groups with Trp189 (Fig. 3G), further confirming the key importance of these aromatic moieties for inhibiting CTSL.

All these investigations highlighted **13** as the lead compound of this series. Then, we questioned whether the inversion of chirality at the carbon bearing the isobutyl moiety (compound **15**) could affect the biological activity. Docking poses highlighted a different binding mode of **15** with respect to **13** and, in particular, the exchange of the positions

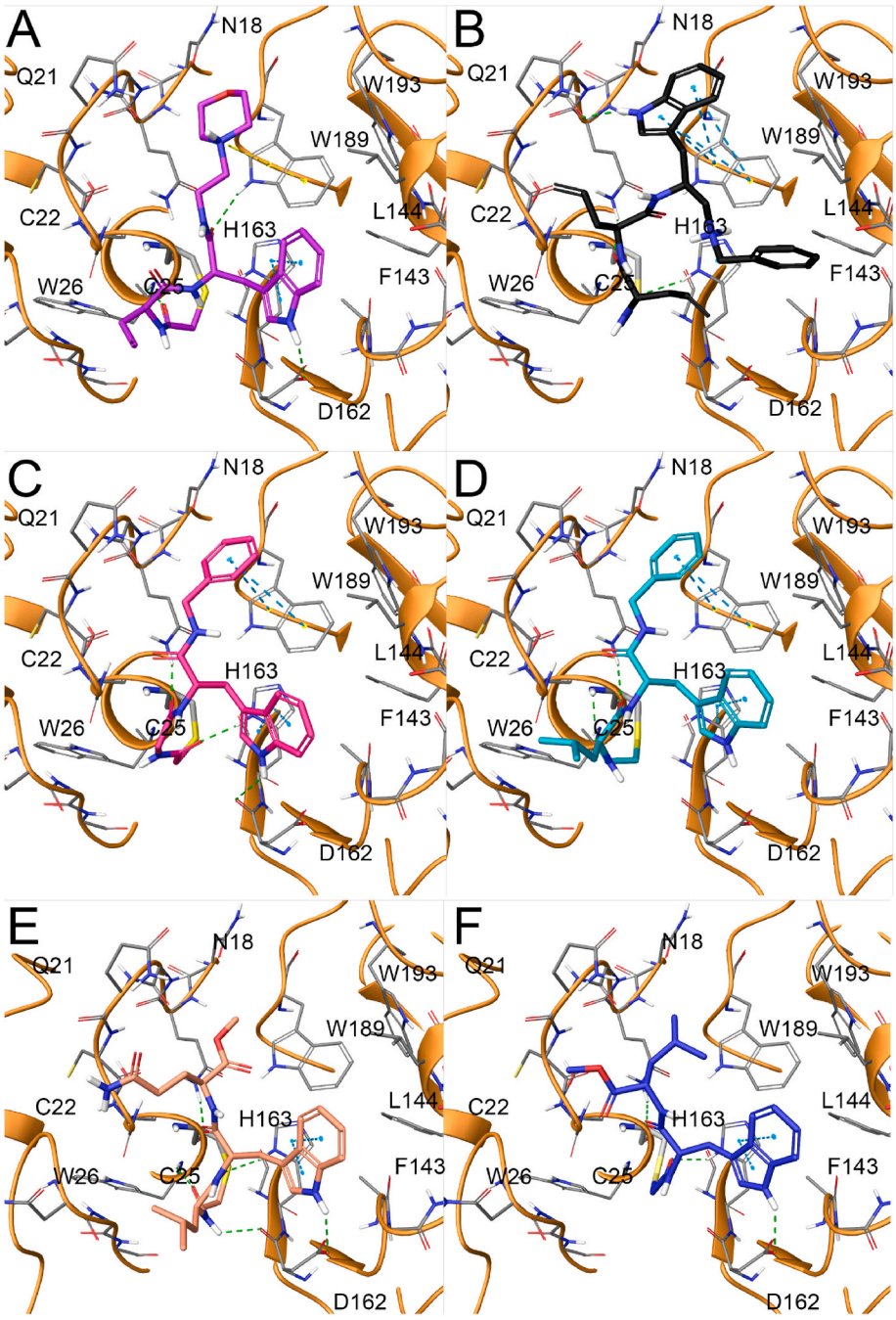

Fig. 3. A) **28** (colored by atom type: C light violet, O red, N blue, polar H light grey), B) **39** (colored by atom type: C black, O red, N blue, polar H light grey); C) **17** (colored by atom type: C purple, O red, N blue, polar H light grey); D) **13** (colored by atom type: C light blue, O red, N blue, polar H light grey); E) **42** (colored by atom type: C salmon, O red, N blue, polar H light grey); F) **33** (colored by atom type: C blue, O red, N blue, polar H light grey); G) **31** (colored by atom type: C dark grey, O red, N blue, polar H light grey); H) **15** (colored by atom type: C light red, O red, N blue, polar H light grey); I) **25** (colored by atom type: C sky blue, O red, N blue, polar H light grey); J) **16** (colored by atom type: C yellow, O red, N blue, polar H light grey); K) **19** (colored by atom type: C violet, O red, N blue, polar H light grey); L) **22** (colored by atom type: C light purple, O red, N blue, polar H light grey); M) **46** (colored by atom type: C light violet, O red, N blue, polar H light grey) in docking with CTSL (secondary structure colored in orange; key residues are reported as sticks and colored by atom type: C grey, O red, N blue, S yellow, polar H light grey). H-bonds and π-π interactions are reported in green and cyan dotted lines, respectively.

of the indole and benzyl moieties in occupying the protein subsites with the subsequent loss of some interactions, in particular the H-bond with Ala138 (Fig. 3H). These data suggested that this chemical variation could affect the biological activity and, indeed, cell-free assays confirmed *in silico* data highlighting an inhibitory effect with 35 times higher IC_{50} than **CV11** (Table 1). Starting again from **13**, we also wondered whether the inversion of the chirality at the carbon bound to the indole moiety and thus close to the benzyl group (compound **25**) could influence the CTSL inhibitory activity. Similarly to **15**, the predicted binding mode was not in line with that sampled for **13** with the lack of π-π and H-bond interactions previously established by **13** (Fig. 3I) and, as expected, the biological results confirmed these data with a marked reduction of the measured inhibitory activity that resulted in a $IC_{50} = 2.92 \pm 0.79$ μM (Table 1).

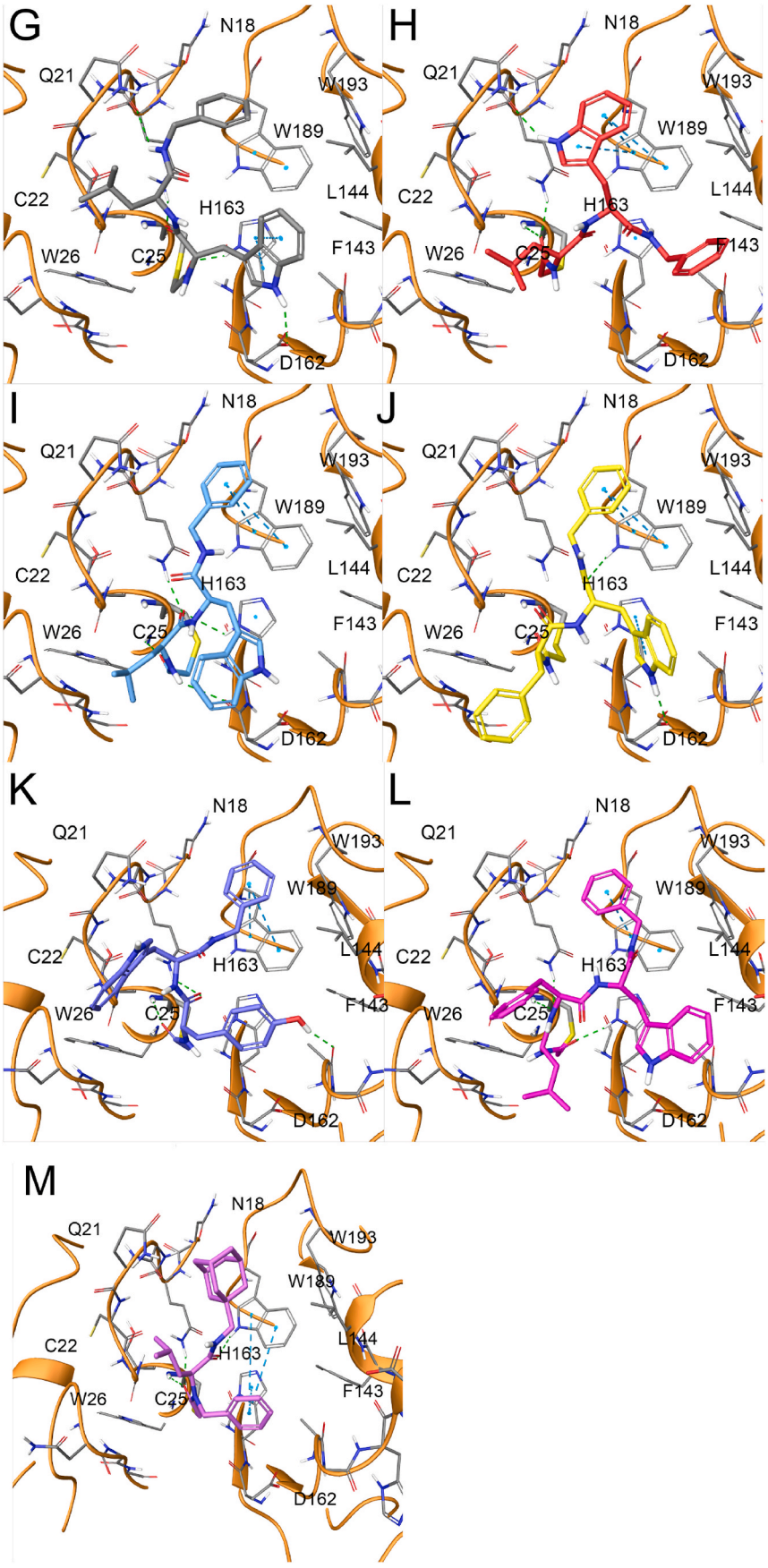

Fig. 3. (*continued*).

Given the importance of the isobutyl moiety occupying S3 subsite, a new set of derivatives was then taken into account by replacing it with a benzyl moiety (compound **16**). In this case, docking results revealed a comparable binding mode between **16** and **13** with the establishment of hydrophobic interactions with residues belonging to S3 subsite (e.g., Asn 66, Gly 67, Gly 68). Also, π-π and H-bond interactions were detected by the indole moiety with His163 and Asp162 and by the benzyl group with Trp189 (Fig. 3I). As expected, biological data were in line with the computational outcomes, disclosing **16** as a very potent inhibitor of CTSL with an IC_{50} of 3.170 ± 0.876 nM (Table 1). However, the replacement of the benzyl moiety with a 4-OH-benzyl in **19** (arising from L-Tyr instead of L-Phe, Scheme 1) highlighted a different orientation of these moieties comparing **16** and **19**. Indeed, the new introduced 4-OH-benzyl is placed in the region occupied by the key indole in **16**, whereas the latter is oriented towards the S2' subsite (Fig. 3J). Biological outcomes highlighted a 16 times reduction of the inhibitory activity (Table 1) in accordance with *in silico* data.

With all these data in hands, we wondered whether the introduction of both the isobutyl and benzyl moieties (present in lead compounds **13** and **16**, respectively) could be beneficial in inhibiting CTSL. In this case, covalent docking calculations were performed for the four possible isomers arising from all the *R/S* configuration combinations (compound **22**, Table 1, and compounds **22a**, **22b**, **22c**, Fig. S33), with the aim of selecting the most promising one. From this analysis, compound **22** showed a binding mode partly respecting the network of interactions previously reported for **13** and **16**, being able to interact with residues belonging to S1, S2, S3, and S1' subsites. In particular, both the close isobutyl and benzyl moieties make the molecule gain additional interactions with residues belonging to S1/S3 subsites, but this is counterbalanced by differently orientation of the indole moiety if compared to **CV11**, **13**, and **16** with the loss of the H-bond with Ala138 and Asp162 (Fig. 3L). *In-vitro* assays confirmed the computational predictions, disclosing **22** as a new potent compound with an IC_{50} comparable to those of **13** and **16**, highlighting the importance of the *S* configuration for all three amino acids composing the tripeptide.

Finally, compounds **14**, **18** and **20** were synthesized as close analogues of the lead compounds **13** and **16**, in which the chloroacetyl moiety was replaced by alkene and thiol functions as putative attachment points for ligand/protein covalent linkage, to provide further evidence of the importance of this group in inhibiting CTSL. As expected, all three items showed a strong decrease in biological activity if compared with **13** and **16** (Table 1), demonstrating that the chloroacetyl is a key pharmacophoric group for developing potent CTSL inhibitors. This outcome was eventually further corroborated by compound **46**, that showed an IC_{50} in the low micromolar range (Table 1) and featured only the chloroacetyl, the benzyl moieties, and the isobutyl as the chosen minimum required groups for inhibiting CTSL, establishing π-π interactions with His163 and Trp189 (Fig. 3M).

All the compounds were also tested as SARS-CoV-2 M^{pro} inhibitors, disclosing **13**, **16**, **19**, **25**, and **31** as able to interfere with this key enzyme with IC_{50} in the high nanomolar/low micromolar ranges of concentrations. Starting from the binding mode of **CV11** against M^{pro} proposed by us [37], we evaluated the new compounds in which the covalent linkage between Cys145 reactive residue [42] and the chloroacetyl moiety was taken into account for molecular docking experiments (Fig. 4). As previously reported [37], **CV11** is able to establish π-π interactions with His41 and a large set of additional hydrophobic contacts, occupying S2, S4, and S1 subsites (Fig. 4A and B). Starting from these premises, we carefully analysed the docking poses of **13**, **16**, **19**, **25**, and **31**, disclosing a binding mode highly compatible with that of **CV11** respecting the same network of interactions and a similar occupation of the above reported M^{pro} subsites (Fig. 5A–E). Interestingly, for compound **25**, the *R* configuration at the carbon bound to the indole moiety instead of *S* configuration as in **13**, **16**, **19**, and **31** led to an inverted occupation of S2/S4 subsites by indole and benzyl moieties (Fig. 5D). Also, compound **31** featured a slightly different accommodation onto the enzyme binding site, specifically regarding the orientation of the indole moiety along the S2 subsite and the arising contacts with His41 (Figs. 5E and 4A).

On the other hand, the analysis of the docking poses related to the inactive compounds featuring the chloroacetyl moiety and the comparison with those related to the active molecules **13**, **16**, **19**, **25**, and **31** disclosed details useful to shed light on the different observed biological behaviours. Indeed, compounds **15**, **17**, **22**, **28**, **33**, **39**, **42**, and **46** are unable to comply with the binding mode observed for the active compounds due to the different occupation of the S1, S2, and S4 subsites (Fig. S34). In details, for most of the inactive molecules, the interactions of the indole moieties towards the S2 subsite were detected but, at the same, the loss of contacts with residues placed in between S4 and S1 subsites (e.g., Phe 140, Glu 166) was observed, providing interesting indications for rationalizing the molecular basis behind the observed biological activities.

2.3. Cell-based pharmacological characterization

Considering the promising enzymatic inhibitory data, we continued our investigations by cell-based assays, using as model Vero cells infected with 5 different variants of SARS-CoV-2. In particular we assessed the capability of our derivatives in decreasing the production of cytopathic effect (CPE) in cells infected with Wuhan, African, UK, Delta and Omicron SARS-CoV-2 variants, using Remdesivir and Molnupinavir as reference drugs. tbl2fnc.

Contextually with this assessment, also the cytotoxic effect of the synthesized compounds has been measured, evaluating the cell morphology (MCC) and the cell growth (CC_{50}). Results are reported in Table 2.

As illustrated in the table, many derivatives exhibited very interesting activity in inhibiting virus growth, showing a remarkable activity also against the omicron variant, currently considered as the most resistant one [20]. Compounds **13**, **15**, **16**, **17**, **19** and **31** appear as the most promising derivatives, in accordance with the enzymatic assays data, resulting in an IC_{50} activity against CTSL between 2.82 ± 0.76 and 100.54 ± 21.46 nM. Moreover, compounds **13**, **16**, **19** and **31**, were also characterized by a micromolar inhibitory potency against M^{pro}. Compounds **25** and **28** presented a moderate antiviral potency, coherently with the enzymatic inhibitory activity for both targets. Differently, the antiviral activity data collected for derivatives **22** and **42**, were not coherent with those deriving from the enzymatic assays, being the compounds highly effective against the CTSL (8.01 ± 2.12 and 82.93 ± 22.67 nM respectively) but almost inactive in the cell evaluation. We justified this incongruency by a possible lack of cell permeability, considering the high molecular weight of these analogues, however other reasons cannot be excluded.

Moreover, most of the tested compounds did not show any cytotoxic effects over a wide panel of cell lines (see Table 2 and Table S3).

2.4. Compounds selectivity

To deepen the compounds biological profile, we performed a wide screening against a panel of different viruses, including α-HCoV (229 E), β-HCoV (OC43), Influenza viruses (H1N1, H3N2, B), Respiratory Syncytial Virus (A Long), Herpes simplex virus 1 (KOS), Yellow fever virus (17D), Sinobis virus (Ar-339), Semliki Forest virus (Original). The obtained results are summarized in Table S3. Many derivatives exhibited an interesting activity against both the HCoVs used (229 E and OC43), while no one worked against the other viruses (Table S3). Except for the compound **19**, all the derivatives exerted an activity against the HCoVs comparable with those recorded against SARS-CoV-2. It is worth noting that the α-HCoV 229 E, as well as the β-HCoV OC43 need the cathepsin L action for being released into the host cells [43]. In addition, the homology degree between the M^{Pro} sequence of SARS-CoV-2 and 229E and OC43 is around 40–50 % [44]. Both these considerations represent a

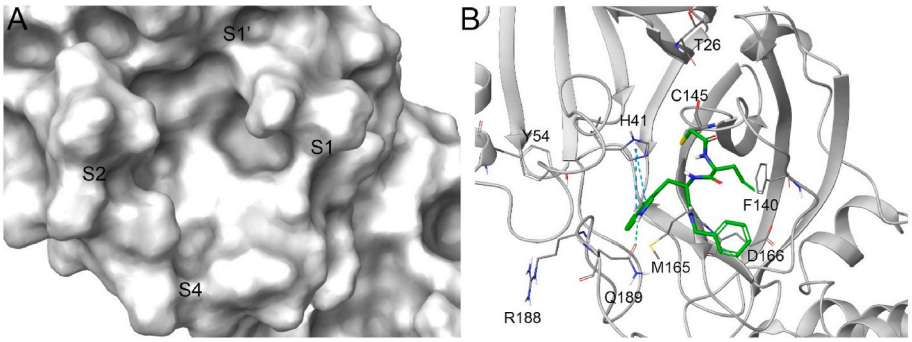

Fig. 4. A) Binding subsites of SARS-CoV-2 M^{pro} enzyme (PDB code: 6M0K). Molecular surface of M^{pro} is depicted in light grey. B) **CV11** (colored by atom type: C green, O red, N blue, polar H light grey) in docking with M^{pro} (secondary structure in ribbons and colored in grey; key residues are reported as sticks and colored by atom type: C grey, O red, N blue, S yellow, polar H light grey). H-bonds and π-π interactions are reported in green and cyan dotted lines, respectively.

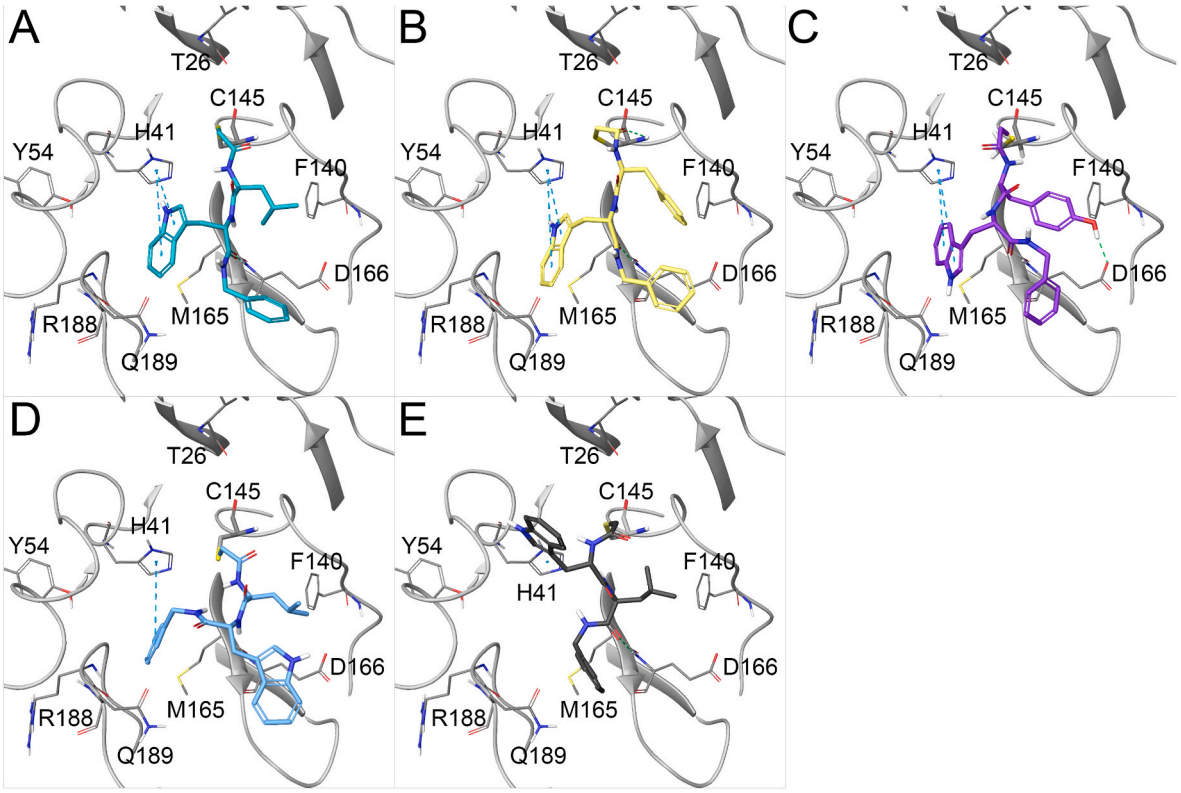

Fig. 5. A) **13** (colored by atom type: C light blue, O red, N blue, polar H light grey); B) **16** (colored by atom type: C yellow, O red, N blue, polar H light grey); C) **19** (colored by atom type: C violet, O red, N blue, polar H light grey); D) **25** (colored by atom type: C sky blue, O red, N blue, polar H light grey); E) **31** (colored by atom type: C dark grey, O red, N blue, polar H light grey) in docking with Sars-CoV-2 M^{pro} (secondary structure colored in grey; key residues are reported as sticks and colored by atom type: C grey, O red, N blue, S yellow, polar H light grey). H-bonds and π-π interactions are reported in green and cyan dotted lines, respectively.

further proof of concept concerning the compounds mechanism of action.

2.5. *In-vitro chemical and metabolic stability*

In this study, we evaluated the chemical and metabolic stability of **13**, **15**, **16**, **17** and, **31** using a LC-MS approach, in order to assess their drug-likeness.

Chemical stability screening is used to assess the degradation of a compound through non-enzymatic processes. Various mechanisms can contribute to the degradation, with the most common ones being hydrolysis, oxidation, or degradation triggered by exposure to light. By subjecting the compounds to different conditions and monitoring their degradation, chemical stability screening provides valuable information on the compound's stability and potential degradation pathways. This information is crucial for evaluating the compound's shelf-life, storage conditions, and overall stability under different environmental conditions.

In this study, chemical stability of **13**, **15**, **16**, **17** and, **31** was evaluated incubating the compounds in SGF and SIF solutions at 37 °C for 120 min. The samples were collected at specific time points and analysed by LC-MS to detect any changes in their chemical structure or composition. Our results highlighted that all investigated compounds were resistant (>80 %) to chemical degradation (Table S2). The same stability was observed when measuring the compound's stability in human plasma at five different time points (Table S2), except for compound **31**, which exhibited a half-life of approximately 24.4 min. Consequently, it was excluded from further investigation.

Table 2
Antiviral activity against SARS-CoV-2 and cytotoxicity in Vero cells.

Compound	SARS-CoV-2 strains EC_{50}[a] (μM)					MCC[b] (μM)	CC_{50}[c] (μM)
	Wuhan	*African*	*UK*	*Delta*	*Omicron*		
Remdesivir	3.74 ± 0.23	2.93 ± 0.00	2.40 ± 1.67	3.74 ± 0.40	0.83 ± 0.05	>40	>40
Molnupiravir	4.31 ± 1.59	5.44 ± 0.00	2.81 ± 0.54	6.04 ± 0.84	1.22 ± 0.14	>100	48.20 ± 25.40
CV11	0.49 ± 0.03	1.16 ± 1.13	0.46 ± 0.32	2.12 ± 0.82	5.87 ± 8.18	>100	>50
13	0.27 ± 0.18	0.32 ± 0.03	0.44 ± 0.16	1.20 ± 0.00	1.28 ± 0.42	>100	>50
14	>100	>100	>100	>100	>100	>100	>50
15	0.08 ± 0.04	0.57 ± 0.25	0.07 ± 0.01	1.08 ± 0.82	1.37 ± 0.93	>100	>50
16	0.09 ± 0.04	0.68 ± 0.66	0.07 ± 0.04	1.30 ± 1.02	1.34 ± 1.42	>100	11.92 ± 3.43
17	0.16 ± 0.10	0.30 ± 0.07	0.07 ± 0.00	0.54 ± 0.20	0.81 ± 0.86	>100	>50
18	>100	>100	>100	>100	>100	>100	>50
19	2.37 ± 0.47	3.46 ± 2.19	3.32 ± 2.31	12.27 ± 3.19	5.04 ± 3.49	>100	>50
20	>20	>20	>20	>20	>20	>100	>50
22	4.81 ± 3.96	>20	>20	>20	>100	>100	>50
25	8.71 ± 6.01	>20	8.93 ± 5.23	>20	>20	>100	>50
28	10.33 ± 0.52	10.72 ± 0.30	5.90 ± 2.19	29.25 ± 2.80	13.50 ± 2.54	>100	>50
31	0.25 ± 0.08	0.41 ± 0.02	0.26 ± 0.13	1.25 ± 0.71	0.40 ± 0.09	20.00 ± 8.30	>50
33	>4	>20	>4	>20	>4	21.00 ± 3.50	30.20 ± 0.87
39	4.29 ± 1.56	2.53 ± 0.00	2.16 ± 0.46	18.05 ± 10.75	15.15 ± 12.98	>100	>50
42	>100	>100	>100	>100	>100	>100	>50
46	>4	>4	>4	>4	>4	19.00 ± 5.80	31.40 ± 1.94

[a] Effective concentration required to reduce virus cytopathic effect (CPE) by 50 %. Virus input was 100 $TCID_{50}$ ((Median Tissue Culture Infectious Dose).
[b] Minimum citotoxic concentration that causes a microscopically detectable alteration of Vero cells morphology.
[c] Cytotoxic concentration required to reduce Vero cell growth by 50 %.

In the next step, we evaluated the stability of **13**, **15**, **16** and **17** at the degradation induced by hepatic metabolic enzymes. In our assay we followed the loss of the test compounds over time under CYP and CYP-UGT-mediated metabolic pathways.

Metabolic stability was assessed by adding NADPH to activate only CYPs in human liver microsomes, and UDPGA and NADPH for the activation of both CYPs and UGTs in the presence of alamethicin. To detect non-specific protein binding or heat instability, the compounds were also incubated without cofactors (negative control). Our results demonstrated that all compounds exhibited not protein binding and were highly stable in the absence of cofactors.

The extent of hepatic metabolism was evaluated by monitoring the remaining percentage of parent compound at different time points and allowed us the determination of different pharmacokinetic parameters such as *in-vitro* $t_{1/2}$, $CLint_{in\text{-}vitro}$ and $CLint_{in\text{-}vivo.}$ (Table S2). *In-vitro* $t_{1/2}$ and CLint of tested compounds after liver microsomes incubation were calculated according to "well stirred" model [45]. Predicted $CLint_{in\text{-}vivo}$ values were determined using human PBSF.

Our results indicated that **13** and **15** derivatives showed comparable metabolic profiles in both the dual-activity system and the conventional incubation (Fig. 6) in which only CYPs were active [($t_{1/2}$ **13**: 29.7 min (CYP) *vs* 21.1 min (CYP-UGT); $t_{1/2}$ **15**: 74.5 min (CYP) *vs* 75.3 min (CYP-UGT)]. This finding confirms that these compounds are primarily metabolized through CYP-mediated pathways. However, **16** and **17** were metabolized by phase I and II reactions, suggesting a higher susceptibility to glucuronidation phase compared to other derivatives [$t_{1/2}$ **16**: 38.3 min (CYP) *vs* 19.6 min (CYP-UGT); $t_{1/2}$ **17**: 346.5 min (CYP) *vs* 121.6 min (CYP-UGT)].

According to the classification by McNaney et al. [46], compounds **13** and **16** are categorized as high clearance compounds ($CLint_{in\text{-}vitro}$ >45 mL min^{-1} kg^{-1}); compound **15** fall into the category of intermediate clearance compounds (15 < $CLint_{in\text{-}vitro}$ <45 mL min^{-1} kg^{-1}), while **17** is classified as a low clearance compounds ($CLint_{in\text{-}vitro}$ <15 mL min^{-1} kg^{-1}).

It is interesting to note the different susceptibility to hepatic metabolism of compounds **13** and **15**. This aspect could be related to the stereoselectivity of drug metabolism. Among all pharmacokinetic process, metabolism is the most stereoselective process due to the involvement of the enzyme systems. Metabolizing enzymes often show a preference for one enantiomer of a chiral drug over the other, resulting in enantioselectivity [47,48].

In our study, compounds **15** showed a half-life value about 3 times longer than its relative stereoisomer.

Overall, this investigation underlines that compound **15** is the most chemically stable derivative (*in-vitro* half-life = 232.3 min), while its analogue **17** is the most resistant to the metabolic transformation (*in-vitro* half-life = 121.6 min).

3. Discussion

Since 2019 the worldwide population has been facing the most tremendous sanitary and social catastrophe of the last century accounted for the SARS-CoV-2 infection. Despite being the worst wave of the pandemic overcame, where the humanity was unprepared for tackling the virus, now there is the necessity to implement the measures needed for a long and constant SARS-CoV-2 permanence. The question whether the virus, by mutations acquisition, could escape from the current therapy and eventually from the acquired immunity, is still on debate. The mutations are a direct consequence of each pandemic because they reflect the intrinsic ability of the viruses to adapt themselves to the surrounding habitat and to escape host defences perpetuating their

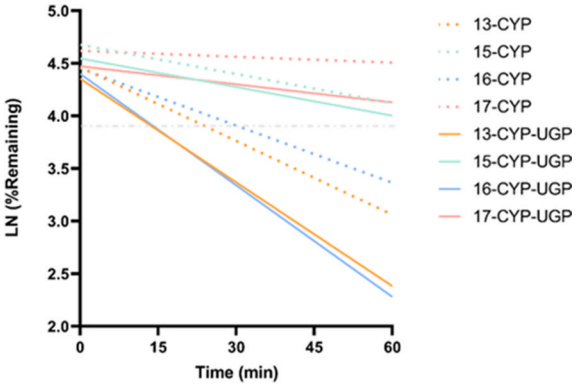

Fig. 6. Representative graph depicting the linear regression of the natural logarithm of % parent compound remaining plotted against incubation time (min). The dotted lines represent the incubation of test compounds in human liver microsomes with only CYPs activated, while solid lines indicate dual activation involving both CYPs and UGTs.

infectious cycle. As a consequence of SARS -CoV-2 long term permanence, mutations are closely related to the recent opinion that COVID-19 is moving toward an endemic infection [49]. This new collocation of the illness, even if it does not make it less dangerous [50], will completely change the global scenario. It will result in a readjustment of all the measures currently fielded, from social behaviour to therapeutic intervention. In fact, the endemization of SARS-CoV-2 will require, besides the achievement of "herd immunity", an appropriate therapy, which must be based on a safer, homely administrated and readily accessible drug arsenal. This prospective enlivens the research endeavour headed for the discovery of potent and selective *anti*-SARS-Cov-2 agents.

In this paper we discuss the design, synthesis, and the antiviral evaluation of a new series of peptidomimetics extremely active against 5 variants of concern of SARS-CoV-2 replication. This study origins from computational evidence about our M^{pro} and PL^{pro} dual inhibitor **CV11**, that showed a potential affinity against CTSL too. This hypothesis has been confirmed by an enzymatic assay in which our lead compound exhibited very high inhibitory activity against CTSL, inspiring the design of a new related series of derivatives. Molecular modelling investigation led to the development of a library of peptidomimetics endowed of remarkable activity against CTSL and some of them also against M^{pro}. The *in-vitro* potency of all the synthesized compounds has been corroborated by cell-based studies performed on Vero cells infected with 5 variants of SARS-CoV-2, including the omicron variant. Compounds **13**, **15**, **16**, **17** and **31**, emerged as the most powerful analogues, in accordance with our previous cell-free evaluation. Moreover, the drug-likeness of the most interesting peptidomimetics was also proved by an *in-vitro* pharmacokinetic assessment, that led to the identification of compound **15** and **17** as the most chemically and metabolically stable derivatives, respectively. It is worth noting that further cell-based analysis highlighted an interesting selectivity of the most promising compounds against other HCoVs, such as 229 E and OC43, underling the potential of these new derivatives. 229E and OC43, differently from SARS-CoV-2, cause milder bronchial infections, because they are limited to the upper respiratory tract and the associated symptomatology is related to local symptoms, mainly represented from cold, for which these viruses are responsible in 15–30 % of cases. To date, no specific pharmacological treatments are available for tackle these infections, that, despite being almost benign, can lead to bronchiolitis and pneumoniae, especially in infants, elderly and immunodeficient patients [51]. This latter point, together with the reported results, enhances the importance of our investigation, highlighting the potential of the developed compounds, that could represent useful tools not only as *anti*-SARS-CoV-2 agents, but also for the treatment of others common viral infections.

4. Experimental section

4.1. Computational details

A starting structural analysis of the CTSL crystal structures co-complexed with inhibitors available in the Protein Data Bank was performed by superposition and comparison through root-mean-square deviation (RMSD) calculation and visual inspection. This analysis highlighted the high structural stability of this enzyme and, accordingly, the protein structure featuring the best resolution (PDB code: 2XU3 [52], namely CTSL in complex with XU3 inhibitor) was chosen for the subsequent molecular docking experiments. Also, 3D structure of SARS-CoV-2 M^{pro} in complex with A1 antagonist (FJC) (PDB code: 6M0K) [53] was taken into account for *in silico* investigations (see Results and Discussion). The above reported protein structures were prepared using the Schrödinger Protein Preparation Wizard workflow [54]. In details, water molecules and the co-complexed compounds were removed, cap termini were included, all hydrogen atoms were added, and bond orders were assigned. The grids considered for the subsequent molecular docking calculations were then generated analyzing the positions of the related co-crystallized compounds.

The investigated compounds (See Results and Discussion) were prepared using LigPrep software (Schrodinger Suite) [55], generating all the possible tautomers and protonation states (pH = 7.4 ± 1.0). Finally, the obtained structures were minimized using the OPLS 2005 force field.

Covalent docking experiments were performed using Glide software (Schrödinger Suite) [56]. Cys25 and Cys145 were set as the reactive residues for CTLS and SARS-CoV-2 M^{pro}, respectively. The specific reaction type (nucleophilic substitution) was selected in the related panel, according to the specific ligand chemical features arising from the presence of the α-chloro ketone moiety (see Results and Discussion). The Virtual Screening mode was chosen as docking mode, setting 2.5 kcal/mol as energy cutoff to retain poses for further refinement and 200 as related number of maximum number of poses to be retained. In the output file, 20 poses for each compound were saved.

5. Enzymatic assays

5.1. M^{pro} enzymatic assay

The assay was performed in a volume of 25 μL in black 384-well OptiPlate. A fluorescent FRET substrate (DABCYL-KTSAVLQSGFRKME-EDANS) harboring the cleavage site of SARS-CoV-2 M^{pro} and aqueous buffer solution (40 mM Tris-HCl, pH 8.0, 110 mM NaCl, 2.2 mM KCl, 20 % glycerol, 3 mM DTT, 8 mM maltose) were used for the inhibition assay (BPS Bioscience 3 C L Protease, MBP-tagged Assay). M^{pro} recombinant protease, at a final concentration of 150 ng per reaction, was pre-incubated for 30 min at room temperature with slow shaking in presence of the compounds at different concentrations. Finally, the reaction was initiated by adding 5 μL of the FRET substrate to each well (final concentration, 50 μM). Buffer with the same amount of DMSO (1 %) was used as control and M^{pro} inhibitor GC376 is also included as a positive control. The plate was covered with a TopSeal™-A PLUS sealing film to prevent contamination and evaporation of the samples and incubated for 4 h at room temperature in subdued light. The fluorescence signals (excitation/emission, 360 nm/460 nm) of released EDANS were read using a PerkinElmer EnSpire multimode plate reader. The experiments were performed in triplicate. The IC_{50} values were calculated using GraphPad Prism 8.0 software by nonlinear regression of dose-response inhibition.

5.2. CTSL enzymatic assay

The assay was performed in a volume of 50 μL in black 96-well OptiPlate. A fluorometric dipeptide Z-Leu-Arg-AMC was used as substrate in CTSL enzymatic assay (BPS Bioscience Cathepsin L Inhibitor Screening Assay Kit). Upon cleavage by CTSL, the fluorescence of the AMC moiety dramatically raises. For steady state measurement, the enzyme was incubated for 10 min at room temperature (final concentration, 25 ng per reaction) with the compounds at different concentrations in cathepsin buffer. Then, the reaction was initiated by adding 25 μL of the substrate to each well (final concentration, 10 μM). Buffer with the same amount of DMSO (1 %) was used as negative control. The CTSL inhibitor E−64 is also included as a positive control. The plate was covered with a TopSeal™-A PLUS sealing film to prevent contamination and evaporation of the samples and incubated in the dark for 60 min at room temperature. The fluorescence signals (excitation/emission, 360 nm/460 nm) were read using a PerkinElmer EnSpire multimode plate reader. The experiments were performed in triplicate. The IC_{50} values were calculated using GraphPad Prism 8.0 software by nonlinear regression of dose-response inhibition.

5.3. Chemistry

All reagents and solvents used were purchased from Sigma-Aldrich (Milan, Italy) unless otherwise stated. 2-Mercaptoacetyl chloride was

purchased from Syntechem Co. Ltd (Shanghai, China). Reactions were performed under magnetic stirring in round-bottom flasks or under microwave irradiation assisted (Biotage, Initiator EU). TLC analysis of reaction mixtures was performed on pre-coated glass silica gel plates (F254, 0.25 mm, VWR International). The crude products were purified by the Isolera Spektra One automated flash chromatography system (Biotage, Uppsala, Sweden), using commercial silica gel cartridges (SNAP KP-Sil, Biotage). NMR spectra were recorded on a Bruker Avance 400 MHz apparatus, at room temperature. Chemical shifts were reported in δ values (ppm) relative to internal Me_4Si for ^1H and ^{13}C NMR. J values were reported in hertz (Hz). ^1H NMR and ^{19}F NMR peaks were described using the following abbreviations: s (singlet), bs (broad singlet), d (doublet), t (triplet), and m (multiplet). HR-MS spectra were recorded by LTQ-Orbitrap-XL-ETD mass spectrometer (Thermo Scientific, Bremen, Germany), equipped with electrospray ionization. Circular dicroism spectra were recorded using a JASCO J810 spectropolarimeter at 25 °C in the range λ 280–220 nm (1 mm path length, 1 nm bandwidth, four accumulations, and a scanning speed of 10 nm/min). Measurements were performed in methanol at concentrations of 0.8 mM. Spectra were corrected for the solvent contribution.

5.4. General procedure A: coupling reaction (1, 3–7, 27, 30, 34, 41, 45)

Boc-*L*-Trp-OH, Boc-*D*-Trp-OH, *Z*-*L*-Trp-OH, **2**, **10**, **23**, **36**, **37**, **44**, deprotected intermediate **26**, **29** or **40** (1 mmol), was dissolved in dichloromethane and added with HOBt (1.2 eq), HBTU (1.2 eq), DIPEA (2.4 eq), and the proper amine (1.2 eq) or carboxylic acid (1.2 eq) and stirred at room temperature overnight. Then, the crude mixture was diluted with dichloromethane and washed with water (3 × 100 mL), a saturated solution of $NaHCO_3$ (3 × 100 mL), and a solution of citric acid (10 % w:w, 3 × 100 mL). The organic layer was extracted, dried over Na_2SO_4, filtered, and concentrated in vacuo. The crude products were purified by flash chromatography using mixtures of *n*-hexane/ethyl acetate as mobile phase.

5.5. General procedure B: Boc removal (2, 8–12, 21, 23, 24, 39, 42)

N-Boc protected intermediate **1, 3–7**, coupled **10,** coupled **D-Trp**, coupled **23**, **26**, **27**, **29**, **30**, coupled **38** or coupled **41** (0.1 mmol) was dissolved in a mixture of TFA/DCM (1/3, v/v), and triisopropylsilane (TIS, 0.25 eq) was added. The reaction mixture was stirred at room temperature for 3 h. After the completion of the reaction, a solution of NaOH (2 N) was added, the mixture was diluted with water and DCM, and the organic phase was extracted twice, dried over Na_2SO_4, filtered, and concentrated under vacuum. The obtained intermediates were used in the next step without further purification.

5.6. General procedure C: acylation reaction (13–20, 22, 25, 28, 31, 33, 46)

Intermediates **8–12, 21, 24, 32, 35, 38**, deprotected **27, 30, 41** or **45** (0.1 mmol) were dissolved in dichlorometane and added with 1.2 eq of TEA and 1.2 eq of chloroacetyl chloride or di-*tert*-butyl dicarbonate. The reaction mixtures were stirred at room temperature for 1 h. After the completion of the reaction, monitored by TLC, the organic phases were washed with a saturated solution of $NaHCO_3$ (3 × 100 mL) and a solution of citric acid (10 % w:w, 3 × 100 mL). The organic layers were extracted, dried over Na_2SO_4, filtered, and concentrated under vacuum. The crude mixtures were purified by flah chromatography using ethyl acetate/methanol as eluent.

5.7. General procedure D: hydrolysis (44)

1.0 mmol of **29** or protected **43** was dissolved in a solution of MeOH and NaOH 2 M and stirred at reflux for 3 h. The reaction was quenched by a 2 M aqueous solution of HCl, and the mixture was extracted three times with ethyl acetate (3 × 50 mL), dried over sodium sulfate, and concentrated under vacuum. The obtained intermediates were used in the next step without further purification.

5.8. General procedure G: Cbz removal (36)

Removal of Cbz protecting group was achieved by continuous flow hydrogenation using the H-Cube hydrogenator and commercially available Pd/C 10 % cartridges as catalyst. Intermediate **35** or **40** was dissolved in a mixture of THF/CH_3OH (1:1, v:v) at a final concentration of 0.1 M and was pumped at a flow rate of 1.0 mL min^{-1}. Temperature was set at 30 °C, while the hydrogen inlet pressure was set at 10 bar. After completion, the reaction mixture was evaporated under vacuum and the obtained products used in the following step without further purification.

5.9. General procedure H: Fmoc removal (37, 38)

Intermediate **36** or **38** was dissolved in a mixture of dichloromethane/diethylamine (3:1 v:v) and stirred at room temperature for 3 h. The organic mixture was added with a saturated solution of $NaHCO_3$, diluted with ethyl acetate, extracted, dried over sodium sulfate and concentrated under vacuum. The obtained reaction mixture was treated with *n*-hexane to precipitate the desired compound as a white powder, without further purification step.

5.10. (S)-tert-butyl (1-(benzylamino)-3-(1H-indol-3-yl)-1-oxopropan-2-yl)carbamate (1)

Synthesized according to the general procedure A, starting from Boc-L-Trp-OH and benzylamine.

FC in *n*-hexane/ethyl acetate 7/3, Rf = 0.45. Yellowish oil (80 % yield). ^1H NMR (400 MHz, CD_3OD): δ: 1.40 (s, 9H, CH_3); 3.10 (dd, 1H, CH_{2a}, J' = 6.6, J'' = 13.8 Hz); 3.25 (dd, 1H, CH_{2b}, J' = 6.9, J'' = 14.4 Hz); 4.19–4.23 (m, 1H, CH); 4.34–4.41 (m, 2H, CH_2); 7.02–7.06 (m, 5H, aryl); 7.12 (t, 1H, aryl, J = 7.1 Hz); 7.20–7.25 (m, 2H, aryl); 7.37 (d, 1H, aryl, J = 8.1 Hz); 7.62 (d, 1H, aryl, J = 7.8 Hz). HR-MS *m/z* calcd for $C_{23}H_{28}N_3O_3$ [(M + H)]+: 394.2125; found 394.2118.

5.11. (S)-2-Amino-N-benzyl-3-(1H-indol-3-yl)propanamide (2)

Intermediate **2** was synthesized according to the general procedure B, starting from **1**. White powder (95 % yield). ^1H NMR (400 MHz, CD_3OD): δ: 3.05 (dd, 1H, CH_{2a}, J' = 5.8, J'' = 10.4 Hz); 3.20 (dd, 1H, CH_{2b}, J' = 6.0, J'' = 10.4 Hz); 3.69 (t, 1H, CH, J = 5.2 Hz); 4.25 (d, 1H, CH_{2a}, J = 12.6 Hz); 4.35 (d, 1H, CH_{2b}, J = 12.6 Hz); 7.02–7.07 (m, 5H, aryl); 7.12 (t, 1H, aryl, J = 7.2 Hz); 7.20–7.26 (m, 2H, aryl); 7.39 (d, 1H, aryl, J = 8.2 Hz); 7.64 (d, 1H, aryl, J = 8.0 Hz). HR-MS *m/z* calcd for $C_{18}H_{20}N_3O$ [(M + H)]+: 294.1601; found 294.1608.

5.12. tert-butyl ((S)-1-(((S)-1-(benzylamino)-3-(1H-indol-3-yl)-1-oxopropan-2-yl)amino)-4-methyl-1-oxopentan-2-yl)carbamate (3)

Intermediate **3** was synthetized starting from **2** and Boc-L-Leu-OH following the general procedure A. FC in hexane/ethyl acetate 1/1, R*f*: 0.47. White powder (75 % yield). ^1H NMR (400 MHz, CD_3OD): δ 0.89 (d, 3H, CH_3, J = 6.5 Hz); 0.93 (d, 3H, CH_3, J = 6.6 Hz); 1.43–1.49 (m, 2H, CH_2); 1.56–1.66 (m, 1H, CH); 3.28 (d, 2H, CH_2, J = 6.4 Hz); 3.99 (t, 1H, CH, J = 7.4 Hz); 4.22 (d, 1H, CH_{2a}, J = 15.0 Hz); 4.32 (d, 1H, CH_{2b}, J = 15.0 Hz); 4.68 (t, 1H, CH, J = 6.3 Hz); 7.02–7.07 (m, 5H, aryl); 7.12 (t, 1H, aryl, J = 7.6 Hz); 7.19–7.24 (m, 2H, aryl); 7.37 (d, 1H, aryl, J = 8.1 Hz); 7.62 (d, 1H, aryl, J = 8.0 Hz). HR-MS *m/z* calcd for $C_{29}H_{38}N_4O_4$ $[(M + H)]^+$: 507.2966; found 507.2960.

5.13. tert-butyl ((S)-1-(((S)-1-(benzylamino)-3-(1H-indol-3-yl)-1-oxopropan-2-yl)amino)-4-methyl-1-oxopentan-2-yl)carbamate (4)

Intermediate **4** was synthetized starting from **2** and Boc-D-Leu-OH following the general procedure A. FC in hexane/ethyl acetate 1/1, R*f*: 0.47. White powder (72 % yield). ^{1}H NMR (400 MHz, DMSO): δ 0.73 (d, 3H, CH_3, J = 6.0 Hz); 0.79 (d, 3H, CH_3, J = 6.1 Hz); 1.13–1.22 (m, 1H, CH); 1.23–1.32 (m, 2H, CH_2); 1.39 (s, 9H, CH_3); 2.93 (dd, 1H, CH_{2a}, J' = 10.0, J'' = 14.5 Hz); 3.00–3.04 (m, 2H, CH_2); 3.23 (dd, 1H, CH_{2b}, J' = 4.5, J'' = 14.5 Hz); 3.97–4.02 (m, 2H, CH); 4.51–4.57 (m, 1H, CH); 6.96 (t, 1H, aryl, J = 7.2 Hz); 7.05 (t, 1H, aryl, J = 7.4 Hz); 7.10 (s, 1H, aryl); 7.13–7.20 (m, 5H, aryl); 7.53 (d, 1H, aryl, J = 7.4 Hz); 7.59 (d, 1H, aryl, J = 7.8 Hz). HR-MS *m/z* calcd for $C_{29}H_{38}N_4O_4$ [(M + H)]$^+$: 507.2966; found 507.2968.

5.14. tert-butyl (1-(((S)-1-(benzylamino)-3-(1H-indol-3-yl)-1-oxopropan-2-yl)amino)-1-oxo-3-phenylpropan-2-yl)carbamate (5)

Intermediate **5** was synthetized starting from **2** and Boc-Phe-OH following the general procedure A. FC in hexane/ethyl acetate 7/3, R*f*: 0.49. White powder (82 % yield). ^{1}H NMR (400 MHz, DMSO): δ 1.29 (s, 9H, 3 CH_3); 1.72–1.75 (m, 2H, CH_2); 2.68–2.74 (m, 1H, CH_{2a}); 2.90 (dd, 1H, CH_{2b}, J' = 10.1, J'' = 14.0 Hz); 3.00–3.16 (m, 2H, CH_2); 4.13–4.19 (m, 1H, CH); 4.24 (d, 2H, CH_2, J = 5.6 Hz); 4.59–4.64 (m, 1H, CH); 6.94 (d, 1H, aryl, J = 8.4 Hz); 6.99 (d, 1H, aryl, J = 7.4 Hz); 7.08 (d, 2H, aryl, J = 7.08 Hz); 7.16–7.24 (m, 8H, aryl); 7.34 (d, 1H, aryl, J = 8.0 Hz); 7.60 (d, 1H, aryl, J = 7.8 Hz); 8.01 (d, 1H, aryl, J = 7.9 Hz); 8.42 (t, 1H, NH, J = 5.6 Hz); 10.85 (s, 1H, N*H*). HR-MS *m/z* calcd for $C_{32}H_{36}N_4O_4$ [(M + H)]$^+$: 541.2809; found 541.2815.

5.15. tert-butyl (S)-(2-((1-(benzylamino)-3-(1H-indol-3-yl)-1-oxopropan-2-yl)amino)-2-oxoethyl)carbamate (6)

Intermediate **6** was synthetized starting from **2** and Boc-Gly-OH following the general procedure A. FC in hexane/ethyl acetate 1/1, R*f*: 0.47. White powder (80 % yield). ^{1}H NMR (400 MHz, CD_3OD): δ 1.37 (s, 3H, CH_3); 3.26 (t, 1H, CH_{2a}, J = 6.1 Hz); 3.33 (d, 1H, CH_{2b}, J = 1.6 Hz); 3.65 (d, 1H, CH_{2a}, J = 16.9 Hz); 3.71 (d, 1H, CH_{2b}, J = 16.9 Hz); 4.25 (d, 1H, CH_{2a}, J = 15.1 Hz); 4.32 (d, 1H, CH_{2b}, J = 15.1 Hz); 4.72 (t, 1H, CH, J = 6.4 Hz); 7.03–7.06 (m, 4H, aryl); 7.12 (t, 1H, aryl, J = 7.1 Hz); 7.19–7.26 (m, 3H, aryl); 7.37 (d, 1H, aryl, J = 8.0 Hz); 7.62 (d, 1H, aryl, J = 7.8 Hz). HR-MS *m/z* calcd for $C_{25}H_{30}N_4O_4$ [(M + H)]$^+$: 451.2340; found 451.2338.

5.16. tert-butyl ((S)-1-(((S)-1-(benzylamino)-3-(1H-indol-3-yl)-1-oxopropan-2-yl)amino)-3-(4-hydroxyphenyl)-1-oxopropan-2-yl) carbamate (7)

Intermediate **7** was synthetized starting from **2** and Boc-L-Tyr-OH following the general procedure A. FC in hexane/ethyl acetate 4/6, R*f*: 0.47. White powder (65 % yield). ^{1}H NMR (400 MHz, CD_3OD): δ 1.31 (s, 9H, CH_3); 2.80 (dd, 1H, CH_{2a}, J' = 8.7, J'' = 13.8 Hz); 2.99 (dd, 1H, CH_{2b}, J' = 5.2, J'' = 13.9 Hz); 3.16–3.30 (m, 2H, CH_2); 4.19–4.23 (m, 2H, CH_{2a} and CH); 4.30 (d, 1H, CH_{2b}, J = 15.1 Hz); 4.68 (t, 1H, CH, J = 6.2 Hz); 6.88 (d, 2H, aryl, J = 8.4 Hz); 7.00–7.05 (m, 4H, aryl); 7.09 (d, 2H, aryl, J = 8.3 Hz); 7.14–7.23 (m, 5H, aryl); 7.37 (d, 1H, aryl, J = 7.9 Hz). HR-MS *m/z* calcd for $C_{32}H_{36}N_4O_5$ [(M + H)]$^+$: 557.2758; found 557.2761.

5.17. (S)-2-Amino-N-((S)-1-(benzylamino)-3-(1H-indol-3-yl)-1-oxopropan-2-yl)-4-methylpentanamide (8)

Intermediate **8** was synthetized starting from **3** following the general procedure B. White powder (93 % yield). ^{1}H NMR (400 MHz, CD_3OD): δ 0.87 (d, 3H, CH_3, J = 6.6 Hz); 0.90 (d, 3H, CH_3, J = 6.6 Hz); 1.22–1.31 (m, 1H, CH_{2a}); 1.40–1.47 (m, 1H, CH_{2b}); 1.56–1.65 (m, 1H, CH); 3.18 (dd, 1H, CH_{2a}, J' = 7.2, J'' = 14.4 Hz); 3.29–3.38 (m, 2H, CH_{2b} and CH, J = 7.4 Hz); 4.25 (d, 1H, CH_{2a}, J = 15.0 Hz); 4.33 (d, 1H, CH_{2b}, J = 15.0 Hz); 4.73 (t, 1H, CH, J = 7.3 Hz); 7.01–7.08 (m, 5H, aryl); 7.12 (t, 1H, aryl, J = 8.0 Hz); 7.20–7.25 (m, 2H, aryl); 7.37 (d, 1H, aryl, J = 8.1 Hz); 7.64 (d, 1H, aryl, J = 7.8 Hz). HR-MS *m/z* calcd for $C_{24}H_{30}N_4O_2$ [(M + H)]$^+$: 407.2442; found 407.2446.

5.18. (R)-2-Amino-N-((S)-1-(benzylamino)-3-(1H-indol-3-yl)-1-oxopropan-2-yl)-4-methylpentanamide (9)

Intermediate **9** was synthetized starting from **4** following the general procedure B. White powder (94 % yield). ^{1}H NMR (400 MHz, CD_3OD): δ 0.77 (t, 6H, CH_3, J = 5.7 Hz); 1.17–1.24 (m, 1H, CH); 1.28–1.35 (m, 2H, CH_2); 3.13 (dd, 1H, CH_{2a}, J' = 8.5, J'' = 14.5 Hz); 3.27 (t, 1H, CH, J = 6.8 Hz); 3.33–3.38 (m, 1H, CH_{2b}); 4.32 (d, 1H, CH_{2a}, J = 15.0 Hz); 4.37 (d, 1H, CH_{2a}, J = 15.0 Hz); 4.77 (dd, 1H, CH, J' = 6.2, J'' = 8.5 Hz); 7.03 (t, 1H, aryl, J = 7.0 Hz); 7.08 (s, 1H, aryl); 7.13 (t, 1H, aryl, J = 6.8 Hz); 7.21–7.29 (m, 2H, aryl); 7.31–7.40 (m, 2H, aryl); 7.64 (d, 1H, aryl, J = 7.9 Hz); 7.74 (d, 1H, aryl, J = 7.5 Hz); 7.79 (d, 1H, aryl, J = 7.6 Hz). HR-MS *m/z* calcd for $C_{24}H_{30}N_4O_2$ [(M + H)]$^+$: 407.2442; found 407.2438.

5.19. (S)-2-Amino-N-((S)-1-(benzylamino)-3-(1H-indol-3-yl)-1-oxopropan-2-yl)-3-phenylpropanamide (10)

Intermediate **10** was synthetized starting from **5** following the general procedure B. White powder (95 % yield). ^{1}H NMR (400 MHz, CD_3OD): δ 3.04 (dd, 1H, CH_{2a}, J' = 8.1, J'' = 14.2 Hz); 3.15–3.26 (m, 3H, CH_{2b} and CH_2); 4.13 (t, 1H, CH, J = 6.2 Hz); 4.21 (d, 1H, CH_{2a}, J = 18.7 Hz); 4.32 (d, 1H, CH_{2b}, J = 18.8 Hz); 4.74 (t, 1H, CH, J = 7.5 Hz); 7.00 (d, 1H, aryl, J = 7.7 Hz); 7.04 (t, 1H, aryl, J = 7.8 Hz); 7.13 (t, 1H, aryl, J = 7.8 Hz); 7.19–7.24 (m, 5H, aryl); 7.26–7.33 (m, 5H, aryl); 7.38 (d, 1H, aryl, J = 7.4 Hz); 7.66 (d, 1H, aryl, J = 7.5 Hz). HR-MS *m/z* calcd for $C_{27}H_{28}N_4O_2$ [(M + H)]$^+$: 441.2285; found 441.2291.

5.20. (S)-2-(2-aminoacetamido)-N-benzyl-3-(1H-indol-3-yl) propanamide (11)

Intermediate **11** was synthetized starting from **6** following the general procedure B. White powder (92 % yield). ^{1}H NMR (400 MHz, CD_3OD): δ 3.16 (dd, 1H, CH_{2a}, J' = 7.4, J'' = 14.4 Hz); 3.30 (dd, 1H, CH_{2b}, J' = 7.2, J'' = 15.1 Hz); 3.63 (d, 1H, CH_{2a}, J = 16.0 Hz); 3.72 (d, 1H, CH_{2b}, J = 16.0 Hz); 4.25 (d, 1H, CH_{2a}, J = 15.0 Hz); 4.33 (d, 1H, CH_{2b}, J = 15.0 Hz); 4.77 (t, 1H, CH, J = 7.3 Hz); 7.02–7.08 (m, 4H, aryl); 7.12 (t, 1H, aryl, J = 7.7 Hz); 7.18–7.25 (m, 3H, aryl); 7.37 (d, 1H, aryl, J = 8.1 Hz); 7.64 (d, 1H, aryl, J = 7.7 Hz). HR-MS *m/z* calcd for $C_{20}H_{22}N_4O_2$ [(M + H)]$^+$: 351.1816; found 351.1824.

5.21. (S)-2-Amino-N-((S)-1-(benzylamino)-3-(1H-indol-3-yl)-1-oxopropan-2-yl)-3-(4-hydroxyphenyl)propanamide (12)

Intermediate **12** was synthetized starting from **7** following the general procedure B. White powder (94 % yield). ^{1}H NMR (400 MHz, CD_3OD): δ 2.74 (dd, 1H, CH_{2a}, J' = 7.6, J'' = 13.9 Hz); 2.94 (dd, 1H, CH_{2b}, J' = 6.2, J'' = 14.3 Hz); 3.14–3.27 (m, 2H, CH_2); 3.70 (t, 1H, CH, J = 5.8 Hz); 4.21 (d, 1H, CH_{2a}, J = 15.0 Hz); 4.33 (d, 1H, CH_{2b}, J = 15.0 Hz); 4.71 (t, 1H, CH, J = 7.2 Hz); 6.74 (d, 2H, aryl, J = 8.5 Hz); 7.01–7.05 (m, 6H, aryl); 7.12 (t, 1H, aryl, J = 7.1 Hz); 7.19–7.25 (m, 3H, aryl); 7.37 (d, 1H, aryl, J = 7.9 Hz); 7.59 (d, 1H, aryl, J = 8.0 Hz). HR-MS *m/z* calcd for $C_{27}H_{28}N_4O_3$ [(M + H)]$^+$: 457.2234; found 457.2229.

5.22. (S)–N-((S)-1-(benzylamino)-3-(1H-indol-3-yl)-1-oxopropan-2-yl)-2-(2-chloroacetamido)-4-methylpentanamide (13)

Derivative **13** was synthetized starting from **8** and chloroacetyl chloride following the general procedure C. FC in ethyl acetate/methanol 9.8/0.2, R*f*: 0.47. Yellowish powder (55 % yield). ^{1}H NMR (400

MHz, CD_3OD): δ: 0.89 (d, 3H, C*H*$_3$, $J = 6.4$ Hz); 0.93 (d, 3H, C*H*$_3$, $J = 6.4$ Hz); 1.53 (t, 2H, C*H*$_2$, $J = 6.8$ Hz); 1.56–1.65 (m, 1H, C*H*); 3.18 (dd, 1H, C*H*$_{2a}$, $J' = 7.0$; $J'' = 14.4$ Hz); 3.28–3.33 (m, 1H, C*H*$_{2b}$); 3.98 (q, 2H, C*H*$_2$, $J = 13.4$ Hz); 4.28 (q, 2H, C*H*$_2$, $J = 13.6$ Hz); 4.40 (t, 1H, C*H*, $J = 7.4$ Hz); 4.69 (t, 1H, C*H*, $J = 7.2$ Hz); 7.01–7.06 (m, 5H, aryl); 7.11 (t, 1H, aryl, $J = 7.2$ Hz); 7.18–7.25 (m, 2H, aryl); 7.36 (d, 1H, aryl, $J = 8.1$ Hz); 7.61 (d, 1H, aryl, $J = 7.8$ Hz).^{13}C NMR (100 MHz, CD_3OD) δ: 20.6, 21.9, 24.4, 27.4, 40.2, 41.6, 42.7, 52.3, 54.4, 109.3, 110.9, 118.0, 118.5, 121.0, 123.3, 126.7, 127.0, 127.4, 128.0, 136.7, 138.0, 168.0, 172.2, 172.6. HR-MS *m/z* calcd for $C_{26}H_{31}ClN_4O_3$ $[(M + H)]^+$: 483.2157; found 483.2108.

5.23. (S)-2-Acrylamido-N-((S)-1-(benzylamino)-3-(1H-indol-3-yl)-1-oxopropan-2-yl)-4-methylpentanamide (14)

Derivative **14** was synthetized starting from **8** and acryloyl chloride following the general procedure C. FC in hexane/ethyl acetate 2/8, R*f*: 0.45. White powder (58 % yield). ^{1}H NMR (400 MHz, DMSO): δ: 0.82 (d, 3H, C*H*$_3$, $J = 6.5$ Hz); 0.86 (d, 3H, C*H*$_3$, $J = 6.5$ Hz); 1.43 (t, 2H, C*H*$_2$, $J = 6.9$ Hz); 1.51–1.57 (m, 1H, C*H*); 3.01 (dd, 1H, C*H*$_{2a}$, $J' = 7.7$, $J'' = 14.6$ Hz); 3.15 (dd, 1H, C*H*$_{2b}$, $J' = 6.2$, $J'' = 14.6$ Hz); 4.17–4.28 (m, 2H, C*H*$_2$); 4.38–4.44 (m, 1H, C*H*); 4.54–4.60 (m, 1H, C*H*); 5.60 (dd, 1H, C*H*$_{2a}$, $J' = 2.2$, $J'' = 10.1$ Hz); 6.09 (dd, 1H, C*H*$_{2b}$, $J' = 2.2$, $J'' = 17.1$ Hz); 6.32 (dd, 1H, C*H*$_{2b}$, $J' = 10.2$, $J'' = 17.1$ Hz); 6.97 (t, 1H, aryl, $J = 7.0$ Hz); 7.06 (t, 1H, aryl, $J = 8.0$ Hz); 7.08–7.11 (m, 1H, aryl); 7.20–7.26 (m, 2H, aryl); 7.33 (d, 1H, aryl, $J = 8.4$ Hz); 7.57 (d, 1H, aryl, $J = 7.8$ Hz); 8.10 (d, 1H, aryl, $J = 8.0$ Hz); 8.22 (d, 1H, aryl, $J = 8.1$ Hz); 8.36 (t, 1H, aryl, $J = 6.0$ Hz).^{13}C NMR (100 MHz, DMSO) δ: 22.0, 23.5, 24.7, 28.1, 41.2, 42.5, 51.6, 54.0, 110.4, 111.7, 118.9, 121.3, 124.0, 126.0, 127.1, 127.4, 127.8, 128.6, 132.0, 136.5, 139.6, 165.0, 171.6, 172.0. HR-MS *m/z* calcd for $C_{27}H_{32}N_4O_3$ $[(M + H)]^+$: 461.2547; found 461.2535.

5.24. (R)-N-((S)-1-(benzylamino)-3-(1H-indol-3-yl)-1-oxopropan-2-yl)-2-(2-chloroacetamido)-4-methylpentanamide (15)

Derivative **15** was synthetized starting from **9** and chloroacetyl chloride following the general procedure C. FC in ethyl acetate/methanol 9.8/0.2, R*f*: 0.44. White powder (48 % yield). ^{1}H NMR (400 MHz, CD_3OD): δ: 0.73 (d, 3H, C*H*$_3$, $J = 6.5$ Hz); 0.76 (d, 3H, C*H*$_3$, $J = 6.5$ Hz); 1.14–1.21 (m, 1H, C*H*); 1.32 (t, 2H, C*H*$_2$, $J = 7.4$ Hz); 3.08 (dd, 1H, C*H*$_{2a}$, $J' = 9.7$, $J'' = 14.6$ Hz); 3.45 (dd, 1H, C*H*$_{2b}$, $J' = 8.3$, $J'' = 14.6$ Hz); 3.92 (q, 2H, C*H*$_2$, $J = 13.5$ Hz); 4.21 (t, 1H, C*H*, $J = 7.6$ Hz); 4.40 (q, 2H, C*H*$_2$, $J = 15.0$ Hz); 4.78 (dd, 1H, C*H*$_{2a}$, $J' = 8.3$, $J'' = 14.6$ Hz); 7.02 (t, 1H, aryl, $J = 7.8$ Hz); 7.08 (s, 1H, aryl); 7.11 (t, 1H, aryl, $J = 7.2$ Hz); 7.23 (t, 3H, aryl, $J = 7.6$ Hz); 7.27–7.31 (m, 2H, aryl); 7.35 (d, 1H, aryl, $J = 8.1$ Hz); 7.62 (d, 1H, aryl, $J = 7.9$ Hz).^{13}C NMR (100 MHz, CD_3OD) δ: 21.0, 21.4, 24.1, 27.2, 39.9, 41.4, 42.7, 52.8, 54.3, 109.6, 110.9, 118.0, 118.5, 121.1, 123.2, 126.7, 127.17, 127.22, 128.0, 136.8, 138.3, 168.0, 172.4, 173.1. HR-MS *m/z* calcd for $C_{26}H_{31}ClN_4O_3$ $[(M + H)]^+$: 483.2157; found 483.2181.

5.25. (S)–N-benzyl-2-((S)-2-(2-chloroacetamido)-3-phenylpropanamido)-3-(1H-indol-3-yl)propenamide (16)

Derivative **16** was synthetized starting from **10** and chloroacetyl chloride following the general procedure C. FC in hexane/ethyl acetate 0.2/9.8, R*f*: 0.42. White powder (68 % yield). ^{1}H NMR (400 MHz, CD_3OD): δ 2.90 (dd, 1H, C*H*$_{2a}$, $J' = 8.4$, $J'' = 13.9$ Hz); 3.07–3.19 (m, 2H, C*H*$_{2b}$ and C*H*$_{2a}$); 3.30 (dd, 1H, C*H*$_{2b}$, $J' = 7.3$, $J'' = 14.4$ Hz); 3.88–3.97 (m, 2H, C*H*$_2$); 4.27 (q, 2H, C*H*$_2$, $J = 15.0$ Hz); 4.59–4.70 (m, 2H, C*H*); 7.01–7.04 (m, 3H, aryl); 7.12 (t, 1H, aryl, $J = 7.3$ Hz); 7.17–7.26 (m, 9H, aryl); 7.37 (d, 1H, aryl, $J = 8.1$ Hz); 7.59 (d, 1H, aryl, $J = 7.9$ Hz).^{13}C NMR (100 MHz, CD_3OD) δ: 27.6, 37.2, 41.5, 42.7, 54.4, 54.9, 109.2, 110.9, 118.0, 118.5, 121.1, 123.4, 126.5, 127.0, 127.4, 128.1, 128.9, 136.5, 138.0, 167.7, 171.2, 172.0. HR-MS *m/z* calcd for $C_{29}H_{29}ClN_4O_3$ $[(M + H)]^+$: 517.2001; found 517.1972.

5.26. (S)–N-benzyl-2-(2-(2-chloroacetamido)acetamido)-3-(1H-indol-3-yl)propanamide (17)

Derivative **17** was synthetized starting from **11** and chloroacetyl chloride following the general procedure C. FC in ethyl acetate, R*f*: 0.45. White powder (63 % yield). ^{1}H NMR (400 MHz, CD_3OD): δ 3.06 (dd, 1H, C*H*$_{2a}$, $J' = 7.0$, $J'' = 14.4$ Hz); 3.16–3.25 (m, 3H, C*H*$_{2b}$ and C*H*$_2$); 3.73 (d, 1H, C*H*$_{2a}$, $J = 16.6$ Hz); 3.81 (d, 1H, C*H*$_{2a}$, $J = 16.6$ Hz); 3.92 (s, 2H, C*H*$_2$); 4.13 (d, 1H, C*H*$_{2a}$, $J = 15.0$ Hz); 4.22 (d, 1H, C*H*$_{2a}$, $J = 15.0$ Hz); 4.60 (t, 1H, C*H*, $J = 7.0$ Hz); 6.90–6.95 (m, 4H, aryl); 7.00 (t, 1H, aryl, $J = 8.0$ Hz); 7.08–7.14 (m, 3H, aryl); 7.25 (d, 1H, aryl, $J = 8.0$ Hz); 7.50 (d, 1H, aryl, $J = 7.9$ Hz).^{13}C NMR (100 MHz, CD_3OD) δ: 27.6, 41.6, 42.4, 42.7, 54.4, 109.2, 110.9, 117.9, 118.5, 121.1, 123.3, 126.6, 127.0, 127.4, 128.0, 136.7, 138.0, 168.5, 169.5, 172.3. HR-MS *m/z* calcd for $C_{22}H_{23}ClN_4O_3$ $[(M + H)]^+$: 427.1531; found 427.1498.

5.27. (S)–N-benzyl-3-(1H-indol-3-yl)-2-((S)-2-(2-mercaptoacetamido)-3-phenylpropanamido)propanamide (18)

Derivative **18** was synthetized starting from **10** and 2-mercaptoacetyl chloride following the general procedure C. FC in ethyl acetate/methanol 9.5/0.5, R*f*: 0.47. White powder (55 % yield). ^{1}H NMR (400 MHz, DMSO): δ 2.55 (t, 1H, C*H*$_{2a}$, $J = 8.0$ Hz); 2.73–2.80 (m, 1H, C*H*$_{2b}$); 2.96–3.02 (m, 2H, C*H*$_{2b}$ and C*H*$_{2a}$); 3.07 (d, 1H, C*H*$_{2a}$, $J = 8.0$ Hz); 3.16 (dd, 1H, C*H*$_{2b}$, $J' = 6.1$, $J'' = 14.4$ Hz); 4.24–4.27 (m, 2H, C*H*$_2$); 4.53–4.64 (m, 2H, C*H*); 6.96–7.00 (m, 1H, aryl); 7.04–7.28 (m, 8H, aryl); 7.34 (d, 1H, aryl, $J = 8.0$ Hz); 7.59–7.62 (m, 1H, aryl); 8.18 (d, 1H, aryl, $J = 8.2$ Hz); 8.24 (t, 1H, aryl, $J = 7.4$ Hz); 8.30 (d, 1H, aryl, $J = 8.0$ Hz); 8.36 (t, 1H, aryl, $J = 5.8$ Hz); 10.84 (s, 1H, N*H*).^{13}C NMR (100 MHz, DMSO) δ: 27.4, 28.4, 38.0, 42.1, 42.5, 54.1, 54.6, 110.3, 111.7, 118.7, 118.9, 121.3, 124.1, 126.7, 127.1, 127.4, 127.8, 128.6, 129.7, 136.6, 137.9, 139.6, 168.1, 169.8, 171.1, 171.6. HR-MS *m/z* calcd for $C_{29}H_{30}N_4O_3S$ $[(M + H)]^+$: 515.2111; found 515.3351.

5.28. (S)–N-benzyl-2-((S)-2-(2-chloroacetamido)-3-(4-hydroxyphenyl)propanamido)-3-(1H-indol-3-yl)propanamide (19)

Derivative **19** was synthetized starting from **11** and chloroacetyl chloride following the general procedure C. FC in ethyl acetate/methanol 9.5/0.5, R*f*: 0.48. White powder (59 % yield). ^{1}H NMR (400 MHz, CD_3OD): δ 2.66 (dd, 1H, C*H*$_{2a}$, $J' = 9.0$, $J'' = 13.8$ Hz); 2.88 (dd, 1H, C*H*$_{2a}$, $J' = 4.6$, $J'' = 13.9$ Hz); 3.00 (dd, 1H, C*H*$_{2a}$, $J' = 7.9$, $J'' = 14.5$ Hz); 3.15 (dd, 1H, C*H*$_{2a}$, $J' = 6.2$, $J'' = 14.6$ Hz); 4.02 (s, 2H, C*H*$_2$); 4.21–4.31 (m, 2H, C*H*$_2$); 4.48–4.53 (m, 1H, C*H*); 4.57–4.62 (m, 1H, C*H*); 6.60 (d, 2H, aryl, $J = 8.4$ Hz); 6.97 (d, 2H, aryl, $J = 8.2$ Hz); 7.05–7.14 (m, 3H, aryl); 7.21–7.28 (m, 2H, aryl); 7.34 (d, 1H, aryl, $J = 8.1$ Hz); 7.61 (d, 1H, aryl, $J = 7.8$ Hz); 8.24 (d, 1H, aryl, $J = 8.2$ Hz); 8.31 (d, 1H, aryl, $J = 8.0$ Hz); 8.36 (t, 1H, aryl, $J = 6.0$ Hz); 9.15 (s, 1H, N*H*); 10.84 (s, 1H, N*H*).^{13}C NMR (100 MHz, CD_3OD) δ: 28.4, 37.3, 42.5, 42.9, 54.1, 54.7, 110.3, 111.7, 115.3, 118.7, 118.9, 121.3, 124.1, 127.1, 127.4, 127.8, 128.6, 130.6, 136.5, 139.6, 156.2, 165.9, 170.9, 171.6. HR-MS *m/z* calcd for $C_{29}H_{29}ClN_4O_4$ $[(M + H)]^+$: 533.1950; found 533.1907.

5.29. N-((S)-1-(((S)-1-(benzylamino)-3-(1H-indol-3-yl)-1-oxopropan-2-yl)amino)-1-oxo-3-phenylpropan-2-yl)acrylamide (20)

Derivative **20** was synthetized starting from **10** and acryloyl chloride following the general procedure C. FC in ethyl acetate, R*f*: 0.45. White powder (48 % yield). ^{1}H NMR (400 MHz, CD_3OD): δ 2.78 (dd, 1H, C*H*$_{2a}$, $J' = 8.7$, $J'' = 14.0$ Hz); 2.98 (dd, 1H, C*H*$_{2b}$, $J' = 5.9$, $J'' = 13.9$ Hz); 3.03–3.17 (m, 2H, C*H*$_2$); 4.11 (d, 1H, C*H*$_{2a}$, $J = 15.0$ Hz); 4.17 (d, 1H, C*H*$_{2b}$, $J = 15.0$ Hz); 4.52–4.57 (m, 2H, C*H*); 5.50 (dd, 1H, C*H*$_a$, $J' = 2.2$, $J'' = 9.8$ Hz); 6.00 (dd, 1H, C*H*$_{2a}$, $J' = 2.2$, $J'' = 17.0$ Hz); 6.08 (dd, 1H, C*H*$_{2b}$, $J' = 9.8$, $J'' = 17.1$ Hz); 6.88–6.92 (m, 3H, aryl); 6.99 (t, 1H, aryl, $J = 7.1$ Hz); 7.05–7.12 (m, 9H, aryl); 7.23 (d, 1H, aryl, $J = 8.1$ Hz); 7.45 (d, 1H, aryl, $J = 7.9$ Hz).^{13}C NMR (100 MHz, CD_3OD) δ: 27.5, 37.1, 42.7,

54.4, 54.9, 109.2, 110.9, 118.0, 118.5, 121.0, 123.3, 126.1, 126.4, 126.6, 127.0, 128.0, 128.8, 129.9, 136.7, 136.8, 138.0, 166.7, 171.75, 171.79. HR-MS *m/z* calcd for $C_{30}H_{30}N_4O_3$ $[(M + H)]^+$: 495.2391; found 495.2346.

5.30. (S)-2-Amino-N-((S)-1-(((S)-1-(benzylamino)-3-(1H-indol-3-yl)-1-oxopropan-2-yl)amino)-1-oxo-3-phenylpropan-2-yl)-4-methylpentanamide (21)

Intermediate **21** was synthetized starting from *tert*-butyl ((R)-1-(((S)-1-(((S)-1-(benzylamino)-3-(1H-indol-3-yl)-1-oxopropan-2-yl)amino)-1-oxo-3-phenylpropan-2-yl)amino)-4-methyl-1-oxopentan-2-yl)carbamate obtained from **10** and Boc-L-Leu-OH according to the general procedure A, following the general procedure B. White powder (78 % yield). ^{1}H NMR (400 MHz, CD_3OD): δ 0.90 (d, 3H, C*H*$_3$, $J = 6.5$ Hz); 0.95 (d, 3H, C*H*$_3$, $J = 6.5$ Hz); 1.63 (t, 2H, C*H*$_2$, $J = 6.6$ Hz); 1.68–1.74 (m, 1H, C*H*); 2.96 (dd, 1H, C*H*$_{2a}$, $J' = 8.6$, $J'' = 14.0$ Hz); 3.09–3.14 (m, 1H, C*H*$_{2b}$); 3.16–3.26 (m, 2H, C*H*$_2$); 3.80 (t, 1H, C*H*, $J = 7.5$ Hz); 4.18 (d, 1H, C*H*$_{2a}$, $J = 15.0$ Hz); 4.28 (d, 1H, C*H*$_{2b}$, $J = 15.0$ Hz); 4.65 (t, 1H, C*H*, $J = 7.5$ Hz); 4.71 (t, 1H, C*H*, $J = 6.4$ Hz); 6.98 (d, 1H, aryl, $J = 7.7$ Hz); 7.03 (t, 1H, aryl, $J = 7.3$ Hz); 7.06 (s, 1H, aryl); 7.12 (t, 1H, aryl, $J = 7.4$ Hz); 7.19–7.24 (m, 9H, aryl); 7.37 (d, 1H, aryl, $J = 8.1$ Hz); 7.61 (d, 1H, aryl, $J = 7.9$ Hz). HR-MS *m/z* calcd for $C_{33}H_{39}N_5O_3$ $[(M + H)]^+$: 554.3126; found 554.3119.

5.31. (S)–N-((S)-1-(((S)-1-(benzylamino)-3-(1H-indol-3-yl)-1-oxopropan-2-yl)amino)-1-oxo-3-phenylpropan-2-yl)-2-(2-chloroacetamido)-4-methylpentanamide (22)

Derivative **22** was synthetized starting from **21** and chloroacetyl chloride following the general procedure C. FC in ethyl acetate/methanol 9.8/0.2, R*f*: 0.44. White powder (52 % yield). ^{1}H NMR (400 MHz, DMSO): δ: 0.81 (d, 3H, C*H*$_3$, $J = 6.5$ Hz); 0.84 (d, 3H, C*H*$_3$, $J = 6.5$ Hz); 1.38 (t, 2H, C*H*$_2$, $J = 7.4$ Hz); 1.48–1.54 (m, 1H, C*H*); 2.80 (dd, 1H, C*H*$_{2a}$, $J' = 9.3$, $J'' = 13.9$ Hz); 2.98–3.04 (m, 2H, C*H*$_{2b}$ and C*H*$_{2a}$); 3.14 (dd, 1H, C*H*$_{2b}$, $J' = 6.7$, $J'' = 14.5$ Hz); 4.06 (q, 2H, C*H*$_2$, $J = 12.9$ Hz); 4.24 (d, 2H, C*H*$_2$, $J = 5.7$ Hz); 4.28–4.34 (m, 1H, C*H*); 4.52–4.61 (m, 2H, C*H*); 6.98 (t, 1H, aryl, $J = 7.1$ Hz); 7.05–7.09 (m, 2H, aryl); 7.13 (s, 1H, aryl); 7.18–7.26 (m, 5H, aryl); 7.35 (d, 1H, aryl, $J = 8.0$ Hz); 7.59 (d, 1H, aryl, $J = 7.8$ Hz); 8.08–8.14 (m, 2H, aryl); 8.24 (d, 1H, aryl, $J = 8.3$ Hz); 8.34 (t, 1H, aryl, $J = 6.0$ Hz); 10.8 (s, 1H, N*H*).^{13}C NMR (100 MHz, DMSO) δ: 22.1, 23.4, 24.6, 28.5, 37.7, 40.3, 40.5, 40.7, 41.3, 42.5, 43.0, 51.8, 54.1, 54.3, 110.2, 111.7, 118.7, 118.9, 121.3, 124.1, 126.7, 127.1, 127.4, 127.8, 128.4, 128.6, 129.7, 136.6, 138.1, 139.5, 166.1, 171.0, 171.5, 171.9. HR-MS *m/z* calcd for $C_{35}H_{40}ClN_5O_4$ $[(M + H)]^+$: 630.2842; found 630.2830.

5.32. (R)-2-Amino-N-benzyl-3-(1H-indol-3-yl)propanamide (23)

Intermediate **23** was synthetized starting from (R)-*tert*-butyl (1-(benzylamino)-3-(1H-indol-3-yl)-1-oxopropan-2-yl)carbamate obtained from **23** and Boc-L-Leu-OH according to the general procedure A, following the general procedure B. White powder (88 % yield). ^{1}H NMR (400 MHz, CD_3OD): δ 3.04 (dd, 1H, C*H*$_{2a}$, $J' = 6.8$, $J'' = 14.1$ Hz); 3.19 (dd, 1H, C*H*$_{2b}$, $J' = 6.7$, $J'' = 14.1$ Hz); 3.67 (t, 1H, C*H*, $J = 6.8$ Hz); 4.22 (d, 1H, C*H*$_{2a}$, $J = 14.9$ Hz); 4.34 (d, 1H, C*H*$_{2a}$, $J = 14.9$ Hz); 7.01–7.05 (m, 4H, aryl); 7.12 (t, 1H, aryl, $J = 7.2$ Hz); 7.19–7.24 (m, 3H, aryl); 7.38 (d, 1H, aryl, $J = 8.0$ Hz); 7.63 (d, 1H, aryl, $J = 7.9$ Hz). HR-MS *m/z* calcd for $C_{18}H_{19}N_3O$ $[(M + H)]^+$: 294.1601; found 294.1597.

5.33. (S)-2-Amino-N-((R)-1-(benzylamino)-3-(1H-indol-3-yl)-1-oxopropan-2-yl)-4-methylpentanamide (24)

Intermediate **24** was synthetized starting from *tert*-butyl ((R)-1-(((R)-1-(benzylamino)-3-(1H-indol-3-yl)-1-oxopropan-2-yl)amino)-4-methyl-1-oxopentan-2-yl)carbamate, obtained from **23** and Boc-L-Leu-OH according to the general procedure A, following the general procedure B. White powder (78 % yield). ^{1}H NMR (400 MHz, CD_3OD): δ 0.71 (d, 3H, C*H*$_3$, $J = 6.4$ Hz); 0.75 (d, 3H, C*H*$_3$, $J = 6.4$ Hz); 1.23–1.30 (m, 3H, C*H* and C*H*$_2$); 3.11 (t, 1H, C*H*$_{2a}$, $J = 14.1$ Hz); 3.48 (dd, 1H, C*H*$_{2b}$, $J' = 4.8$, $J'' = 14.6$ Hz); 3.90 (t, 1H, C*H*, $J = 7.4$ Hz); 4.34 (d, 1H, C*H*$_{2a}$, $J = 15.0$ Hz); 4.45 (d, 1H, C*H*$_{2a}$, $J = 14.8$ Hz); 4.81–4.84 (m, 1H, C*H*); 7.02 (t, 1H, aryl, $J = 7.7$ Hz); 7.07 (s, 1H, aryl); 7.10 (t, 1H, aryl, $J = 7.2$ Hz); 7.19–7.28 (m, 5H, aryl); 7.35 (d, 1H, aryl, $J = 8.1$ Hz); 7.63 (d, 1H, aryl, $J = 7.9$ Hz). HR-MS *m/z* calcd for $C_{24}H_{30}N_4O_2$ $[(M + H)]^+$: 407.2442; found 407.2445.

5.34. (S)–N-((R)-1-(benzylamino)-3-(1H-indol-3-yl)-1-oxopropan-2-yl)-2-(2-chloroacetamido)-4-methylpentanamide (25)

Derivative **25** was synthetized starting from **24** and chloroacetyl chloride following the general procedure C. FC in ethyl acetate/methanol 9.8/0.2, R*f*: 0.45. White powder (52 % yield). ^{1}H NMR (400 MHz, CD_3OD): δ: 0.73 (d, 3H, C*H*$_3$, $J = 6.5$ Hz); 0.76 (d, 3H, C*H*$_3$, $J = 6.5$ Hz); 1.14–1.21 (m, 1H, C*H*); 1.32 (t, 2H, C*H*$_2$, $J = 7.4$ Hz); 3.08 (dd, 1H, C*H*$_{2a}$, $J' = 9.7$, $J'' = 14.6$ Hz); 3.45 (dd, 1H, C*H*$_{2b}$, $J' = 8.3$, $J'' = 14.6$ Hz); 3.92 (q, 2H, C*H*$_2$, $J = 13.5$ Hz); 4.21 (t, 1H, C*H*, $J = 7.6$ Hz); 4.40 (q, 2H, C*H*$_2$, $J = 15.0$ Hz); 4.78 (dd, 1H, C*H*$_{2a}$, $J' = 8.3$, $J'' = 14.6$ Hz); 7.03 (t, 1H, aryl, $J = 7.8$ Hz); 7.08 (s, 1H, aryl); 7.11 (t, 1H, aryl, $J = 7.2$ Hz); 7.23 (t, 3H, aryl, $J = 7.6$ Hz); 7.27–7.30 (m, 2H, aryl); 7.35 (d, 1H, aryl, $J = 8.1$ Hz); 7.62 (d, 1H, aryl, $J = 7.9$ Hz).^{13}C NMR (100 MHz, CD_3OD) δ: 21.0, 21.4, 24.1, 27.2, 39.9, 41.4, 42.7, 52.8, 54.3, 109.6, 110.9, 118.0, 118.5, 121.0, 123.2, 126.7, 127.16, 127.22, 128.0, 136.8, 138.3, 168.0, 172.4, 173.1. HR-MS *m/z* calcd for $C_{26}H_{31}ClN_4O_3$ $[(M + H)]^+$: 483.2157; found 483.2138.

5.35. tert-butyl (S)-(3-(1H-indol-3-yl)-1-((2-morpholinoethyl)amino)-1-oxopropan-2-yl)carbamate (26)

Intermediate **26** was synthetized starting from Boc-L-Trp-OH and 4-(2-aminoethyl)morpholine following the general procedure A. FC in ethyl acetate, R*f*: 0.48. Whitish oil (74 % yield). ^{1}H NMR (400 MHz, CD_3OD): δ 1.42 (s, 9H, CH_3); 2.24–2.29 (m, 2H, CH_2); 2.36 (bs, 4H, CH_2); 3.09–3.26 (m, 6H, CH_2); 2.87–2.94 (m, 2H, CH_2); 3.60 (bs, 4H, CH_2); 4.29 (t, 1H, C*H*, $J = 6.8$ Hz); 7.03 (t, 1H, aryl, $J = 7.0$ Hz); 7.09–7.13 (m, 2H, aryl); 7.35 (d, 1H, aryl, $J = 8.0$ Hz); 7.59 (d, 1H, aryl, $J = 7.9$ Hz). HR-MS *m/z* calcd for $C_{22}H_{32}N_4O_4$ $[(M + H)]^+$: 417.2496; found 417.2499.

5.36. tert-butyl ((S)-1-(((S)-3-(1H-indol-3-yl)-1-((2-morpholinoethyl)amino)-1-oxopropan-2-yl)amino)-1-oxobut-3-en-2-yl)carbamate (27)

Intermediate **27** was synthetized starting from (S)-2-amino-3-(1H-indol-3-yl)-*N*-(2-morpholinoethyl)propenamide obtained from **26** according to the general procedure B, and Boc-allyl-Gly-OH following the general procedure A. FC in ethyl acetate/methanol 9.6/0.4, R*f*: 0.47. Whitish oil (58 % yield). ^{1}H NMR (400 MHz, CD_3OD): δ 1.40 (s, 9H, CH_3); 2.12–2.22 (m, 2H, CH_2); 2.24–2.36 (m, 4H, CH_2); 2.45–2.51 (m, 1H, CH_{2a}); 3.07–3.14 (m, 1H, CH_{2b}); 3.18–3.27 (m, 2H, CH_2); 3.58 (t, 4H, CH_2, $J = 4.6$ Hz); 4.04 (dd, 1H, C*H*, $J' = 5.1$, $J'' = 8.4$ Hz); 4.59 (t, 1H, C*H*, $J = 6.6$ Hz); 5.06–5.13 (m, 2H CH_2); 5.68–5.76 (m, 1H C*H*); 7.04 (t, 1H, aryl, $J = 7.6$ Hz); 7.12 (d, 1H, aryl, $J = 8.0$ Hz); 7.15 (s, 1H, aryl); 7.35 (d, 1H, aryl, $J = 8.1$ Hz); 7.60 (d, 1H, aryl, $J = 7.8$ Hz). HR-MS *m/z* calcd for $C_{26}H_{37}N_5O_5$ $[(M + H)]^+$: 500.2867; found 500.2867.

5.37. (S)–N-((S)-3-(1H-indol-3-yl)-1-((2-morpholinoethyl)amino)-1-oxopropan-2-yl)-2-(2-chloroacetamido)pent-4-enamide (28)

Derivative **28** was synthetized starting from (S)–*N*-((S)-3-(1H-indol-3-yl)-1-((2-morpholinoethyl)amino)-1-oxopropan-2-yl)-2-aminopent-4-enamide obtained from **27** according to the general procedure B, and chloroacetyl chloride following the general procedure C. FC in ethyl

acetate/methanol 9.5/0.5, R*f*: 0.47. White powder (52 % yield). ^{1}H NMR (400 MHz, CD_3OD): *δ*: 2.35–2.40 (m, 1H, C*H*$_{2a}$); 2.45–2.51 (m, 1H, C*H*$_{2b}$); 3.04–3.14 (m, 4H, C*H*$_2$); 3.24–3.37 (m, 8H, C*H*$_2$); 3.39–3.44 (m, 1H, C*H*$_{2a}$); 3.56–3.62 (m, 1H, C*H*$_{2b}$); 4.13 (s, 2H, C*H*$_2$); 4.31 (dd, 1H, C*H, J'* = 5.5; *J"* = 8.3 Hz); 4.52 (t, 1H, C*H, J* = 7.4 Hz); 5.04–5.11 (m, 2H, C*H*$_2$); 5.62–5.72 (m, 1H, C*H*); 7.06 (t, 1H, aryl, *J* = 7.7 Hz); 7.13 (t, 1H, aryl, *J* = 8.0 Hz); 7.19 (s, 1H, aryl); 7.38 (d, 1H, aryl, *J* = 8.1 Hz); 7.61 (d, 1H, aryl, *J* = 7.8 Hz).^{13}C NMR (100 MHz, CD_3OD) *δ*: 26.6, 33.6, 35.2, 41.8, 52.1, 54.0, 55.1, 56.5, 63.6, 109.2, 111.1, 117.7, 118.0, 118.6, 121.2, 123.5, 127.4, 132.7, 136.7, 168.5, 172.1, 173.5. HR-MS *m/z* calcd for $C_{24}H_{32}ClN_5O_4$ $[(M + H)]^+$: 490.2216; found 490.2165.

5.38. Methyl (tert-butoxycarbonyl)-L-tryptophyl-L-leucinate (29)

Intermediate **29** was synthetized starting from Boc-L-Trp-OH and L-Leu-OMe following the general procedure A. FC in hexane/ethyl acetate 7/3, R*f*: 0.47. Whitish oil (77 % yield). ^{1}H NMR (400 MHz, $CDCl_3$): *δ* 0.83–0.89 (m, 6H, C*H*$_3$); 1.42–1.54 (m, 12H, C*H*$_3$ and C*H*$_2$ and C*H*); 3.18–3.24 (m, 2H, C*H*$_2$); 3.62 (s, 3H, C*H*$_3$); 4.47–4.46 (m, 2H, C*H*); 5.30 (bs, 1H, N*H*); 6.46 (bs, 1H, N*H*); 4.29 (t, 1H, C*H*, *J* = 6.8 Hz); 7.04 (s, 1H, aryl); 7.08 (t, 1H, aryl, *J* = 7.8 Hz); 7.16 (t, 1H, aryl, *J* = 7.2 Hz); 7.33 (d, 1H, aryl, *J* = 8.0 Hz); 7.63 (d, 1H, aryl, *J* = 7.8 Hz); 8.83 (s, 1H, N*H*). HR-MS *m/z* calcd for $C_{23}H_{33}N_3O_5$ $[(M + H)]^+$: 432.2493; found 432.2489.

5.39. tert-butyl ((S)-1-(((S)-1-(benzylamino)-4-methyl-1-oxopentan-2-yl)amino)-3-(1H-indol-3-yl)-1-oxopropan-2-yl)carbamate (30)

Intermediate **30** was synthetized starting from (*tert*-butoxycarbonyl)-L-tryptophyl-L-leucine obtained from **29** according to general procedure D, and benzylamine following the general procedure A. FC in hexane/ethyl acetate 1/1, R*f*: 0.47. White powder (58 % yield). ^{1}H NMR (400 MHz, CD_3OD): *δ* 0.87–0.92 (m, 6H, C*H*$_3$); 1.19–1.27 (m, 2H, C*H*$_2$); 1.32–1.38 (m, 10H, C*H*$_3$ and C*H*); 3.07–3.12 (m, 1H, C*H*$_{2a}$); 3.23–3.28 (m, 1H, C*H*$_{2b}$); 4.24–4.34 (m, 2H, C*H*$_2$); 4.39–4.42 (m, 2H, C*H*); 4.29 (t, 1H, C*H*, *J* = 6.8 Hz); 7.01–7.12 (m, 4H, aryl); 7.23–7.35 (m, 4H, aryl); 7.61 (d, 1H, aryl, *J* = 7.0 Hz); 7.96 (d, 1H, aryl, *J* = 7.9 Hz). HR-MS *m/z* calcd for $C_{29}H_{38}N_4O_4$ $[(M + H)]^+$: 507.2966; found 507.2960.

5.40. (S)–N-benzyl-2-((S)-2-(2-chloroacetamido)-3-(1H-indol-3-yl) propanamido)-4-methylpentanamide (31)

Derivative **31** was synthetized starting from (S)-2-((S)-2-amino-3-(1H-indol-3-yl)propanamido)-*N*-benzyl-4-methylpentanamide obtained from **30** according to the general procedure B, and chloroacetyl chloride following the general procedure C. FC in hexane/ethyl acetate 2/8, R*f*: 0.47. White powder (48 % yield). ^{1}H NMR (400 MHz, CD_3OD): *δ*: 0.88 (d, 3H, C*H*$_3$, *J* = 6.0 Hz); 0.91 (d, 3H, C*H*$_3$, *J* = 6.0 Hz); 1.56–1.58 (m, 3H, C*H*$_2$ and C*H*); 3.18 (dd, 1H, C*H*$_{2a}$, *J'* = 7.3, *J"* = 14.6 Hz); 3.29–3.35 (m, 1H, C*H*$_{2b}$); 4.02 (dd, 2H, C*H*$_2$, *J'* = 13.8; *J"* = 16.6 Hz); 4.29 (dd, 2H, C*H*$_2$, *J'* = 15.0; *J"* = 20.4 Hz); 4.41 (t, 1H, C*H, J* = 6.1 Hz); 4.73 (t, 1H, C*H, J* = 6.8 Hz); 7.03 (t, 1H, aryl, *J* = 7.0 Hz); 7.09–7.12 (m, 2H, aryl); 7.23–7.25 (m, 3H, aryl); 7.29–7.34 (m, 3H, aryl); 7.60 (d, 1H, aryl, *J* = 6.3 Hz).^{13}C NMR (100 MHz, CD_3OD) *δ*: 20.6, 22.0, 24.3, 27.3, 40.4, 41.7, 42.6, 52.0, 54.5, 109.0, 111.0, 118.0, 118.6, 121.2, 123.3, 126.8, 127.0, 127.2, 128.1, 136.6, 138.4, 167.8, 172.1, 172.9. HR-MS *m/z* calcd for $C_{26}H_{31}ClN_4O_3$ $[(M + H)]^+$: 483.2157; found 483.2121.

5.41. Methyl L-tryptophyl-L-leucinate (32)

Intermediate **32** was synthetized starting from **29** following the general procedure B. White powder (88 % yield). ^{1}H NMR (400 MHz, CD_3OD): *δ* 0.93–0.98 (m, 6H, C*H*$_3$); 1.22–1.26 (m, 2H, C*H*$_2$); 1.63–1.68 (m, 1H, C*H*); 3.20–3.27 (m, 1H, C*H*$_{2a}$); 3.48 (dd, 1H, C*H*$_{2b}$, *J'* = 5.9, *J"* = 14.9 Hz); 3.70 (s, 3H, C*H*$_3$); 4.20–4.25 (m, 1H, C*H*); 4.53 (t, 1H, C*H*, *J* = 7.2 Hz); 7.08 (t, 1H, aryl, *J* = 7.0 Hz); 7.16 (t, 1H, aryl, *J* = 7.9 Hz); 7.26 (s, 1H, aryl); 7.40 (d, 1H, aryl, *J* = 8.1 Hz); 7.70 (d, 1H, aryl, *J* = 7.8 Hz). HR-MS *m/z* calcd for $C_{18}H_{25}N_3O_3$ $[(M + H)]^+$: 332.1969; found 332.1965.

5.42. Methyl (2-chloroacetyl)-L-tryptophyl-L-leucinate (33)

Derivative **33** was synthetized starting from **32** and chloroacetyl chloride following the general procedure C. FC in hexane/ethyl acetate 2/8, R*f*: 0.47. White powder (66 % yield). ^{1}H NMR (400 MHz, CD_3OD): *δ*: 0.90 (d, 3H, C*H*$_3$, *J* = 6.2 Hz); 0.93 (d, 3H, C*H*$_3$, *J* = 6.3 Hz); 1.57–1.68 (m, 3H, C*H*$_2$ and C*H*); 3.16 (dd, 1H, C*H*$_{2a}$, *J'* = 7.4, *J"* = 14.7 Hz); 3.30–3.35 (m, 1H, C*H*$_{2b}$); 3.67 (s, 3H, C*H*$_3$); 4.02 (dd, 2H, C*H*$_2$, *J'* = 13.8; *J"* = 15.8 Hz); 4.48 (t, 1H, C*H, J* = 7.9 Hz); 4.75 (t, 1H, C*H, J* = 6.4 Hz); 7.03 (t, 1H, aryl, *J* = 7.1 Hz); 7.10 (t, 1H, aryl, *J* = 8.1 Hz); 7.14 (s, 1H, aryl); 7.34 (d, 1H, aryl, *J* = 8.0 Hz); 7.62 (d, 1H, aryl, *J* = 7.9 Hz).^{13}C NMR (100 MHz, CD_3OD) *δ*: 20.5, 21.8, 24.4, 27.5, 40.1, 41.7, 50.8, 51.2, 54.2, 109.0, 110.8, 117.9, 118.4, 121.0, 123.4, 127.5, 136.6, 167.4, 172.1, 172.9. HR-MS *m/z* calcd for $C_{20}H_{26}ClN_3O_4$ $[(M + H)]^+$: 408.1685; found 408.1715.

5.43. Benzyl (S)-(3-(1H-indol-3-yl)-1-(methoxy (methyl)amino)-1-oxopropan-2-yl)carbamate (34)

Intermediate **34** was synthetized starting from *Z*-L-Trp-OH and N,O-dimethylhydroxylamine hydrochloride following the general procedure A. FC in hexane/ethyl acetate 7/3, R*f*: 0.47. Whitish oil (85 % yield). ^{1}H NMR (400 MHz, $CDCl_3$): *δ* 3.19–3.25 (m, 4H, C*H*$_3$ and C*H*$_{2a}$); 3.40–3.48 (m, 1H, C*H*$_{2b}$); 3.64 (s, 3H, C*H*$_3$); 5.07–5.18 (m, 2H, C*H*$_2$); 6.03 (d, 1H, C*H, J* = 7.6 Hz); 6.97 (s, 1H, aryl); 7.17–7.26 (m, 2H, aryl); 7.34–7.37 (m, 5H, aryl); 7.70 (d, 1H, aryl, *J* = 7.9 Hz); 9.00 (s, 1H, N*H*). HR-MS *m/z* calcd for $C_{21}H_{23}N_3O_4$ $[(M + H)]^+$: 382.1761; found 382.1758.

5.44. Synthesis of benzyl (S)-(1-(benzylamino)-3-(1H-indol-3-yl) propan-2-yl)carbamate (35)

Intermediate **34** (0.1 mmol) was dissolved in dry THF under nitrogen atmosphere and the temperature was set at 0 °C. The mixture was added with 2.5 eq of 1 M $LiAlH_4$ solution in THF and stirred for 6 min. Then, the crude was quenched with a solution of citric acid (10 % w:w), diluted with DCM, extracted three times, dried over sodium sulfate, and concentrated under vacuum. The obtained aldehyde intermediate was dissolved in dry MeOH under a positive nitrogen flux at room temperature, then benzylamine (1.2 eq) was added. The mixture was stirred at room temperature for 12 h, then $NaBH_4$ (3 eq) was added. After 30 min the organic phase was quenched with a solution of citric acid (10 % w:w), concentrated in vacuo, diluted with ethyl acetate and extracted (3 × 100 mL). The obtained mixture was dried over sodium sulfate, concentrated under vacuum and purified by flash chromatography using mixture of *n*-hexane/ethyl acetate (4:1 v:v) as mobile phase, R*f*: 0.45. Whitish oil (52 % yield). ^{1}H NMR (400 MHz, $CDCl_3$): *δ* 2.38–2.53 (m, 2H, C*H*$_{2a}$ and C*H*$_{2a}$); 2.67–2.81 (m, 2H, C*H*$_{2b}$ and C*H*$_{2b}$); 3.32 (d, 1H, C*H*$_{2a}$, *J* = 12.9 Hz); 3.43 (d, 1H, C*H*$_{2b}$, *J* = 12.9 Hz); 3.99 (bs, 1H, C*H*); 4.85 (s, 2H, C*H*$_2$); 6.80 (s, 1H, aryl); 6.86 (t, 1H, aryl, *J* = 7.1 Hz); 6.92–7.07 (m, 10H, aryl); 7.18 (d, 2H, aryl, *J* = 7.9 Hz); 7.47 (d, 1H, aryl, *J* = 7.7 Hz);. HR-MS *m/z* calcd for $C_{26}H_{27}N_3O_2$ $[(M + H)]^+$: 414.2176; found 414.2178.

5.45. tert-butyl (S)-(2-amino-3-(1H-indol-3-yl)propyl) (benzyl) carbamate (36)

Intermediate **36** was synthetized starting from (S)-(1-(benzyl (*tert*-butoxycarbonyl)amino)-3-(1H-indol-3-yl)propan-2-yl) obtained from **35** using the general procedure C, following the general procedure G. FC in hexane/ethyl acetate 1/1, R*f*: 0.47. White powder (88 % yield). ^{1}H NMR (400 MHz, CD_3OD): *δ* 1.45 (s, 9H, C*H*$_3$); 2.71 (dd, 1H, C*H*$_{2a}$, *J'* = 7.4, *J"* = 14.2 Hz); 2.85–2.89 (m, 1H, C*H*$_{2b}$); 3.30–3.35 (m, 4H, C*H*$_2$); 3.36–3.42 (m, 1H, C*H*); 7.01 (t, 1H, aryl, *J* = 7.6 Hz); 7.05 (s, 1H, aryl);

7.10–7.14 (m, 3H, aryl); 7.23–7.29 (m, 3H, aryl); 7.36 (d, 1H, aryl, J = 7.7 Hz); 7.48 (d, 1H, aryl, J = 7.6 Hz). HR-MS *m/z* calcd for $C_{23}H_{29}N_3O_2$ $[(M + H)]^+$: 380.2333; found 380.2230.

5.46. tert-butyl ((S)-2-((S)-2-aminobut-3-enamido)-3-(1H-indol-3-yl) propyl) (benzyl)carbamate (37)

Intermediate **37** was synthetized from *tert*-butyl ((S)-2-((S)-2-((((9H-fluoren-9-yl)methoxy)carbonyl)amino)but-3-enamido)-3-(1H-indol-3-yl)propyl) (benzyl)carbamate, obtained from **36** and Fmoc-L-allyl Gly-OH using the general procedure A, following the general procedure H. Yellowish powder (78 % yield). ^{1}H NMR (400 MHz, CD_3OD): δ 1.37 (s, 9H, CH_3); 2.15–2.23 (m, 1H, CH_{2a}); 2.26–2.31 (m, 1H, CH_{2b}); 3.42–3.50 (m, 1H, CH); 4.07–4.19 (m, 2H, CH_2); 4.31–4.42 (m, 2H, CH_2); 4.50–4.54 (m, 1H, CH); 4.95 (d, 1H, CH_{2a}, J = 10.6 Hz); 5.02–5.10 (m, 2H, CH_{2b} and CH); 7.00–7.03 (m, 2H, aryl); 7.09 (t, 1H, aryl, J = 7.9 Hz); 7.27–7.32 (m, 2H, aryl); 7.34–7.39 (m, 2H, aryl); 7.56–7.62 (m, 2H, aryl); 7.77 (t, 1H, aryl, J = 7.8 Hz). HR-MS *m/z* calcd for $C_{27}H_{34}N_4O_3$ $[(M + H)]^+$: 463.2704; found 463.2700.

5.47. tert-butyl ((2 S)-2-((2 S)-2-(2-aminobut-3-enamido)but-3-enamido)-3-(1H-indol-3-yl)propyl) (benzyl)carbamate (38)

Intermediate **38** was synthetized from *tert*-butyl ((8*S*, 11*S*)-11-((1H-indol-3-yl)methyl)-1-(9H-fluoren-9-yl)-3,6,9-trioxo-5,8-divinyl-2-oxa-4,7,10-triazadodecan-12-yl) (benzyl)carbamate, obtained from **37** and Fmoc-L-allyl Gly-OH using the general procedure A, following the general procedure H. Yellowish powder (72 % yield). ^{1}H NMR (400 MHz, CD_3OD): δ 1.41 (s, 9H, CH_3); 2.14–2.24 (m, 1H, CH_{2a}); 2.29–2.39 (m, 1H, CH_{2b}); 2.87–2.94 (m, 2H, CH_2); 3.27 (t, 2H, CH_2, J = 7.0 Hz); 3.47–3.58 (m, 1H, CH); 4.16–4.27 (m, 1H, CH); 4.43–4.51 (m, 1H, CH); 5.00–5.10 (m, 2H, CH_{2a}); 5.53–5.68 (m, 4H, CH_{2b} and CH); 7.01–7.05 (m, 3H, aryl); 7.11 (t, 1H, aryl, J = 8.0 Hz); 7.18–7.23 (m, 4H, aryl); 7.35 (d, 1H, aryl, J = 8.2 Hz); 7.60 (t, 1H, aryl, J = 8.1 Hz). HR-MS *m/z* calcd for $C_{31}H_{39}N_5O_4$ $[(M + H)]^+$: 546.3075; found 546.3079.

5.48. (S)–N-((S)-1-(benzylamino)-3-(1H-indol-3-yl)propan-2-yl)-2-((S)-2-(2-chloroacetamido)pent-4-enamido)pent-4-enamide (39)

Derivative **39** was synthetized starting from *tert*-butyl benzyl ((S)-2-((S)-2-((S)-2-(2-chloroacetamido)pent-4-enamido)pent-4-enamido)-3-(1H-indol-3-yl)propyl)carbamate obtained from **38** and chloroacetyl chloride according to procedure C, following the general procedure B. White powder (78 % yield). ^{1}H NMR (400 MHz, CD_3OD): δ: 2.36–2.59 (m, 4H, CH_2); 2.81–2.86 (m, 2H, CH_2); 2.95 (dd, 1H, CH_{2a}, J' = 7.3; J'' = 14.5 Hz); 3.00 (dd, 1H, CH_{2b}, J' = 6.3; J'' = 14.5 Hz); 3.69 (d, 1H, CH_{2a}, J = 12.8 Hz); 3.82 (d, 1H, CH_{2b}, J = 12.8 Hz); 4.11 (s, 2H, CH_2); 4.30 (t, 1H, CH, J = 6.1 Hz); 4.36 (t, 1H, CH, J = 6.5 Hz); 4.42–4.49 (m, 1H, CH); 4.98–5.18 (m, 4H, CH_2); 5.64–5.83 (m, 2H, CH_2); 7.04 (t, 1H, aryl, J = 7.8 Hz); 7.09–7.13 (m, 2H, aryl); 7.23–7.31 (m, 5H, aryl); 7.35 (d, 1H, aryl, J = 7.9 Hz); 7.62 (d, 1H, aryl, J = 8.0 Hz).^{13}C NMR (100 MHz, CD_3OD) δ: 28.2, 35.5, 41.7, 49.1, 51.2, 52.3, 53.8, 110.4, 110.9, 117.4, 117.7, 118.0, 118.4, 121.0, 122.9, 127.2, 127.6, 128.1, 128.5, 129.4, 132.8, 132.2, 136.7, 168.3, 171.9. HR-MS *m/z* calcd for $C_{30}H_{36}ClN_5O_3$ $[(M + H)]^+$: 550.2579; found 550.2523.

5.49. Methyl (S)-2-((S)-2-(((benzyloxy)carbonyl)amino)-3-(1H-indol-3-yl)propanamido)-6-oxo-6-(tritylamino)hexanoate (40)

Intermediate **40** was synthetized starting from *Z*-L-Trp-OH and L-Gln (Trt)-OMe following the general procedure A. FC in hexane/ethyl acetate 1/1, R*f*: 0.47. Whitish oil (72 % yield). ^{1}H NMR (400 MHz, CD_3OD): δ 1.75–1.83 (m, 1H, CH_{2a}); 2.03–2.13 (m, 1H, CH_{2b}); 2.25–2.32 (m, 1H, CH_{2a}); 2.34–2.43 (m, 1H, CH_{2b}); 3.12 (dd, 1H, CH_{2a}, J' = 7.7, J'' = 14.5 Hz); 3.14 (dd, 1H, CH_{2b}, J' = 6.4, J'' = 14.5 Hz); 3.64 (s, 3H, CH_3); 4.43 (t, 1H, CH, J = 5.9 Hz); 4.89–4.94 (m, 2H, CH and CH_{2a}); 4.96 (d, 1H, CH_{2b}, J = 12.5 Hz); 7.00 (t, 1H, aryl, J = 7.2 Hz); 7.09 (t, 1H, aryl, J = 7.2 Hz); 7.19–7.29 (m, 21H, aryl); 7.34 (d, 1H, aryl, J = 8.4 Hz); 7.59 (d, 1H, aryl, J = 8.8 Hz). HR-MS *m/z* calcd for $C_{45}H_{44}N_4O_6$ $[(M + H)]^+$: 737.3334; found 737.3331.

5.50. Methyl (5S,8S,11S)-8-((1H-indol-3-yl)methyl)-1-(9H-fluoren-9-yl)-5-isobutyl-3,6,9-trioxo-11-(4-oxo-4-(tritylamino)butyl)-2-oxa-4,7,10-triazadodecan-12-oate (41)

Intermediate **41** was synthetized starting from methyl (S)-2-((S)-2-amino-3-(1H-indol-3-yl)propanamido)-6-oxo-6-(tritylamino)hexanoate obtained from **40** using the general procedure G, following the general procedure A. FC in hexane/ethyl acetate 3/7, R*f*: 0.47. Whitish oil (68 % yield). ^{1}H NMR (400 MHz, CD_3OD): δ 0.83 (d, 3H, CH_3, J = 6.6 Hz); 0.88 (d, 3H, CH_3, J = 6.6 Hz); 1.20–1.29 (m, 1H, CH_{2a}); 1.35–1.41 (m, 1H, CH_{2b}); 1.48–1.60 (m, 1H, CH); 1.74–1.84 (m, 1H, CH_{2a}); 2.03–2.09 (m, 1H, CH_{2b}); 2.29–2.35 (m, 2H, CH_2); 3.18 (dd, 1H, CH_{2a}, J' = 7.8, J'' = 14.5 Hz); 3.27–3.33 (m, 1H, CH_{2b}); 3.64 (s, 3H, CH_3); 4.03 (t, 1H, CH, J = 7.5 Hz); 4.15 (t, 1H, CH, J = 9.4 Hz); 4.24 (d, 2H, CH_2, J = 7.6 Hz); 4.37–4.41 (m, 1H, CH); 4.64 (t, 1H, CH, J = 6.9 Hz); 6.99 (t, 1H, aryl, J = 7.2 Hz); 7.06 (t, 1H, aryl, J = 7.7 Hz); 7.11 (s, 1H, aryl); 7.15–7.25 (m, 16H, aryl); 7.30 (t, 2H, aryl, J = 7.4 Hz); 7.40 (t, 2H, aryl, J = 7.5 Hz); 7.56 (d, 1H, aryl, J = 7.9 Hz); 7.61 (t, 2H, aryl, J = 7.2 Hz); 7.81 (d, 2H, aryl, J = 7.5 Hz). HR-MS *m/z* calcd for $C_{58}H_{59}N_5O_7$ $[(M + H)]^+$: 938.4487; found 938.4495.

5.51. Methyl (2-chloroacetyl)-L-leucyl-L-tryptophyl-L-glutaminate (42)

Derivative **42** was synthetized starting from methyl N2-(2-chloroacetyl)-L-leucyl-L-tryptophyl-N5-trityl-L-glutaminate, which was obtained from **41**, previously subjected to Fmoc deprotection according to the general procedure H and acylation reaction with chloroacetyl chloride according to the procedure C, following the general procedure B. White powder (38 % yield). ^{1}H NMR (400 MHz, CD_3OD): δ: 0.88 (d, 3H, CH_3, J = 6.4 Hz); 0.92 (d, 3H, CH_3, J = 6.4 Hz); 1.51 (t, 2H, CH_2, J = 8.2 Hz); 1.58–1.63 (m, 1H, CH); 1.86–1.96 (m, 1H, CH_{2a}); 2.09–2.29 (m, 3H, CH_2 and CH_{2b}); 3.19 (dd, 1H, CH_{2a}, J' = 7.8, J'' = 14.7 Hz); 3.29–3.36 (m, 1H, CH_{2b}); 3.68 (s, 3H, CH_3); 4.01 (q, 2H, CH_2, J = 13.4 Hz); 4.36–4.43 (m, 1H, CH); 4.67 (t, 1H, CH, J = 6.4 Hz); 7.03 (t, 1H, aryl, J = 7.4 Hz); 7.10 (t, 1H, aryl, J = 7.8 Hz); 7.14 (s, 1H, aryl); 7.35 (d, 1H, aryl, J = 8.0 Hz); 7.60 (d, 1H, aryl, J = 7.9 Hz).^{13}C NMR (100 MHz, CD_3OD) δ: 20.5, 21.9, 24.4, 27.0, 31.0, 40.1, 41.6, 48.0, 51.4, 51.8, 52.3, 54.2, 109.2, 110.9, 117.9, 118.4, 121.0, 123.4, 127.5, 136.6, 168.0, 171.8, 172.5, 172.7, 176.2. HR-MS *m/z* calcd for $C_{25}H_{34}ClN_5O_6$ $[(M + H)]^+$: 536.2270; found 536.2289.

5.52. Synthesis of methyl benzyl-L-leucinate (43)

L-Leu-OMe was dissolved in dry MeOH under a positive nitrogen flux at room temperature, then benzaldehyde (1.2 eq) was added. The mixture was stirred at room temperature for 12 h, then $NaBH_4$ (3 eq) was added. After 30 min the organic phase was quenched with a solution of citric acid (10 % w:w), concentrated in vacuo, diluted with ethyl acetate and extracted (3 × 100 mL). The obtained mixture was dried over sodium sulfate, concentrated under vacuum and purified by flash chromatography using *n*-hexane/ethyl acetate (8:2 v:v) as mobile phase, R*f*: 0.45. Whitish oil (72 % yield). ^{1}H NMR (400 MHz, CD_3OD): δ 0.85 (d, 3H, CH_3, J = 6.6 Hz); 0.92 (d, 3H, CH_3, J = 6.6 Hz); 1.50 (t, 2H, CH_2, J = 8.5 Hz); 1.66–1.74 (m, 1H, CH); 3.30 (t, 1H, CH, J = 7.2 Hz); 3.61 (d, 1H, CH_{2a}, J = 13.0); 3.71 (s, 3H, CH_3); 3.78 (d, 1H, CH_{2b}, J = 13.0); 7.23–7.33 (m, 5H, aryl). HR-MS *m/z* calcd for $C_{14}H_{21}NO_2$ $[(M + H)]^+$: 235.1572; found 235.1566.

5.53. N-benzyl-N-(tert-butoxycarbonyl)-L-leucine (44)

Intermediate **44** was synthetized starting from methyl *N*-benzyl-*N*-

(*tert*-butoxycarbonyl)-L-leucinate, obtained from methyl benzyl-L-leucinate and di-*tert*-butyl dicarbonate according to the general procedure C, following the general procedure D. White powder (38 % yield). ^{1}H NMR (400 MHz, CD_3OD): δ 0.64 (d, 3H, C*H*$_3$, J = 6.2 Hz); 0.77 (d, 3H, C*H*$_3$, J = 6.2 Hz); 1.50–1.60 (m, 11H, C*H*$_2$ and C*H*$_3$); 1.63–1.72 (m, 1H, C*H*); 4.20 (t, 1H, C*H*, J = 6.1 Hz); 4.28 (d, 1H, C*H*$_{2a}$, J = 14.2); 4.41 (d, 1H, C*H*$_{2b}$, J = 14.0); 7.23–7.33 (m, 5H, aryl). HR-MS *m/z* calcd for $C_{18}H_{27}NO_4$ $[(M + H)]^+$: 322.2013; found 322.2017.

5.54. tert-butyl ((S)-1-((((3S,5S,7S)-adamantan-1-yl)methyl)amino)-4-methyl-1-oxopentan-2-yl) (benzyl)carbamate (45)

Intermediate **45** was synthetized starting from **44** and 1-adamantanemethylamine following the general procedure A. FC in hexane/ethyl acetate 7/3, R*f*: 0.47. Whitish oil (68 % yield). ^{1}H NMR (400 MHz, CD_3OD): δ 0.89 (d, 6H, C*H*$_3$, J = 6.2 Hz); 1.42 (bs, 6H, C*H*$_2$); 1.48 (s, 9H, C*H*$_3$); 1.66 (d, 3H, C*H*$_2$ and C*H*$_{2b}$, J = 11.4 Hz); 1.77 (d, 3H, C*H*$_2$ and C*H*$_{2b}$, J = 11.4 Hz); 1.96 (bs, 3H, C*H*); 2.78–2.86 (m, 2H, C*H*$_2$); 4.39 (d, 1H, C*H*$_{2a}$, J = 15.1); 4.43 (d, 1H, C*H*$_{2b}$, J = 14.9); 4.60 (bs, 1H, C*H*); 7.23–7.34 (m, 5H, aryl). HR-MS *m/z* calcd for $C_{29}H_{44}N_2O_3$ $[(M + H)]^+$: 469.3425; found 469.3422.

5.55. (S)–N-(((3S,5S,7S)-adamantan-1-yl)methyl)-2-(N-benzyl-2-chloroacetamido)-4-methylpentanamide (46)

Derivative **46** was synthetized starting from (S)–*N*-(((3*S*,5*S*, 7*S*)-adamantan-1-yl)methyl)-2-(benzylamino)-4-methylpentanamide obtained from **45** according to the general procedure B, and chloroacetyl chloride following the general procedure C. FC in hexane/ethyl acetate 7/3, R*f*: 0.47. White powder (38 % yield). ^{1}H NMR (400 MHz, $CDCl_3$): δ: 0.87 (d, 3H, C*H*$_3$, J = 6.7 Hz); 0.90 (d, 3H, C*H*$_3$, J = 6.6 Hz); 1.39–1.58 (bs, 8H, C*H*$_2$); 1.64 (d, 3H, C*H*$_2$ and C*H*$_{2a}$, J = 11.8 Hz); 1.73 (d, 3H, C*H*$_2$ and C*H*$_{2b}$, J = 12.0 Hz); 1.89–2.00 (m, 4H, C*H*); 2.90 (dd, 1H, C*H*$_{2a}$, J' = 6.0, J'' = 13.4 Hz); 2.98 (dd, 1H, C*H*$_{2b}$, J' = 6.5, J'' = 13.4 Hz); 3.98 (s, 2H, C*H*$_2$); 4.66–4.77 (m, 2H, C*H*$_2$); 5.00 (dd, 1H, C*H*, J' = 6.2, J'' = 8.4 Hz); 6.43 (bs, 1H, N*H*); 7.20 (d, 2H, aryl, J = 7.4 Hz); 7.32 (d, 1H, aryl, J = 7.1 Hz); 7.36–7.40 (m, 2H, aryl).^{13}C NMR (100 MHz, $CDCl_3$) δ: 22.3, 22.6, 22.9, 25.2, 28.2, 31.6, 33.7, 37.0, 40.2, 41.8, 48.5, 51.0, 57.2, 128.8, 127.7, 129.1, 136.8, 168.9, 170.2. HR-MS *m/z* calcd for $C_{26}H_{37}ClN_2O_2$ $[(M + H)]^+$: 445.2616; found 445.2565.

5.56. SARS-CoV-2 antiviral assay

The Vero cell line (ATCC-CCL81) was used to evaluate the activity of the different compounds against SARS-CoV-2. Cells were grown in Dulbecco's Modified Eagle's Medium (DMEM, ThermoFisher, Belgium) supplemented with 10 % fetal bovine serum (FBS), 2 mM L-glutamine, 0.1 mM non-essential amino acids, 1 mM sodium pyruvate and 10 mM HEPES at 37 °C in a 5 % CO2 humidified atmosphere. The SARS-CoV-19 variant, denoted UC-1074 was isolated in Vero cells (ATCC-CCL81) in 2020 from a nasopharyngeal swab of a COVID-19 patient who had a Ct of 19 for detection of SARS-CoV-2 E protein by RT-qPCR real-time reverse transcription PCR (RT-qPCR). The UC-1074 shares the same genome sequence as the early lineage A sequences (Wuhan/WH04/2020). Four variants of concern, kindly provided by Piet Maes (Laboratory of Clinical and Epidemiological Virology, Rega Institute, KU Leuven, Belgium) were used: NVDBB-2220 (Alpha variant), RG-2674 (Beta variant), 860-J1 (Delta variant) and B1.1.529 B A.1 (Omicron). All variants were used after 2–3 passages in cell culture. The infectious virus titers of the different variants were determined in Vero cells and expressed as 50 % tissue culture infectious dose ($TCID_{50}$) per ml.

The cytopathic effect (CPE) reduction assay was used to evaluate the *anti*-SARS-CoV-2 activity of the compounds. Vero cells were seeded in 96-well plates at a density of 5×10^4 cells per well in DMEM 10 % FBS medium. After 4–5 days of growth, the cell culture medium was removed from the Vero cells grown to confluence, and cells were treated with 5-fold serial dilutions of the compounds diluted in fresh medium (DMEM 2 % FBS) and were then mocked-infected or infected with 100 $TCID_{50}$/well of the SARS-CoV-2 variants (final volume 200 μL/well). The starting drug concentrations of the compounds was 100 μM. Remdisivir, β-D-N^4-hydroxycytidine (NHC; EIDD-1931) and molnupiravir were used as reference *anti*-SARS-CoV-2 compounds. After 6–7 days of incubation at 35 °C, viral CPE was recorded microscopically based on detectable alterations of the cell morphology as soon as it reached completion in the untreated, virus-infected cells, using a 0 to 5 scale (with 0, being no CPE; 1, ~20 % CPE; 2, 20–40 % CPE; 3, ~40–60 % CPE; 4, 60–80 %; and 5, 80–100 % CPE). The 50 % effective concentration (EC_{50}), defined as the drug concentration that reduced the CPE by 50 % compared to the untreated controls, was calculated for each compound from a non-linear curve fit using Prism 4.0 b software.

In parallel, the cytotoxic effects of the derivatives were assessed by evaluating the MCC (minimum cytotoxic concentration that causes a microscopically detectable alteration of cell morphology). The effects of the compounds on cell growth were as well determined by counting the number of cells with a Coulter counter in mock-infected cultures and expressed as the cytostatic concentration required to reduce cell growth by 50 % (CC_{50}). All SARS-CoV-2-related work was conducted in the BSL3 facilities of the KU Leuven Rega Institute (3CAPS) under licenses AMV 30112018 SBB 219 2018 0892 and AMV 23102017 SBB 219 2017 0589 according to institutional guidelines.

5.57. Antiviral activity against different viruses other than SARS-CoV-2

The inhibitory activity of the newly synthesized derivatives was tested against a wide variety of viruses, using the following cell-based assays: (a) human embryonic lung (HEL299) cells: herpes simplex virus-1 (KOS), human coronavirus (229 E and OC43), (b) HeLa cell cultures: respiratory syncytial virus (RSV); (c) Vero cell cultures: Sindbis virus, Semliki Forest virus, yellow fever virus and (d) MDCK cell cultures: influenza A virus (H1N1 and H3N2 subtypes) and influenza B virus. Remdesivir, chloroquine, ribavirin, zanamivir, rimantadine, brivudine, dextran sulfate (molecular weight 10,000), and Aloxistatin (E64d), a cysteine protease inhibitor, were used as reference compounds. Confluent cell cultures in microtiter 96-well plates were inoculated with 100 TCID50 of virus (1 TCID50 being the virus dose to infect 50 % of the cell cultures) and the cell cultures were incubated in the presence of varying concentrations of the test compounds. Viral cytopathic effect was recorded as soon as it reached completion in the control virus-infected cell cultures that were not treated with the test compounds. The antiviral activity was expressed as the EC_{50}: the compound concentration required to reduce virus-induced cytopathogenicity by 50 %. The cytotoxicity of the tested compounds toward uninfected HEL299, HeLa, Vero and MDCK cells was defined as the minimum cytotoxic concentration (MCC) that causes a microscopically detectable alteration of normal cell morphology. The 50 % cytotoxic concentration (CC_{50}), causing a 50 % decrease in cell viability was determined using a colorimetric 3-(4,5-dimethylthiazol-2-yl)-5-(3-carboxymethoxy-phenyl)-2-(4-sulfophenyl)-2H-tetrazolium (MTS) assay system.

6. Instrumentation and analytical conditions

6.1. Instrumentation

RP-UHPLC-PDA MS analysis were performed using a Nexera UHPLC system (Shimadzu, Kyoto, Japan) consisting of a CBM-40 lite controller, two LC-40 B X3 pumps, a CTO-30 A column oven and, a SIL-40C X3 autosampler. The system was coupled online to a Single quadrupole mass spectrometer LCMS 2020 (Shimadzu, Kyoto, Japan) equipped with an Electrospray Ionization (ESI) source.

6.2. LC-MS conditions

All additives and mobile phases were LCMS grade and purchased from Merck (Milan, Italy).

The separation was performed on a Acquity UPLC® CSH ™ C18 100 × 2.1 mm × 1.7 μm (Waters, Milan, Italy) employing as mobile phases: A) H_2O and B) ACN, both acidified with 0.1 % formic acid with the following gradient: 0.01–8.00 min, 5–95 % B, 8.00–10.00 min, isocratic to 95 % B for 2 min, then 5 min for ri-equilibration column. The flow rate and column oven were set at 0.3 mL min^{-1} and 40 °C, respectively.

The ESI was operated in positive mode, with the following parameters: event time: 0.05 s; interface temperature, DL temperature, Heat Block temperature were set to 350 °C, 250 °C and 200 °C, respectively. Nebulizing gas and drying gas flow were set to 1.5 and 15 L min^{-1}, respectively.

MS analyses were conducted in scheduled single reaction monitoring (SIM) employing as precursor [M+H]+ for **13**, **15** and, **31**: 484 *m/z*, **16**: 518 *m/z* and, **17**: 427 *m/z*.

For the calibration curves, the primary stock solutions (10 mM) were prepared in DMSO. The intermediate stock solutions (0.1 mM) and the working standard solutions were prepared by serial dilution of the stock solutions in methanol to obtain necessary concentrations (1–20 μM). Diclofenac acid was used as the internal standard (IS, 296 *m/z*). Quantitation of **13**, **15**, **16**, **17** and **31** compounds was performed using linear regression of the response ratios (peak area analyte/peak area internal standard) obtained from the calibration curve to calculate the corresponding amount.

The following method validation parameters were evaluated: specificity and selectivity, LOD, LOQ, precision and, accuracy.

Specificity and selectivity parameters were evaluated by analysing blank matrix samples from different batches to assess the potential interference of endogenous components in the samples. Chromatograms of these blank matrix samples were compared with chromatograms of matrix samples spiked with a very low concentration of the compound of interest.

Limits of detection (LOD) and quantification (LOQ) were calculated by using the standard deviation (SD) and the slope of the calibration curve, multiplied by 3.3 and 10, respectively. The repeatability of the chromatographic system was assessed in terms of intra-day and inter-day precision. The accuracy was calculated by the percentage relative error (Er %), and the precision was evaluated by the percentage of relative standard deviation (% RSD). The obtained data demonstrated acceptable accuracy and precision of the developed analytical method (Table S1).

6.3. Chemical stability

2.5 μL of test compounds (10 μM final incubation concentration) was incubated in 250 μL of simulated gastric fluid (SGF) or simulated intestinal fluid (SIF) up to 120 min at 37 °C [57].

At each specified time-point (0, 0.5, 1, 1.5 and, 2 h), test compounds were removed into 200 μL ice-cold methanol containing IS to stop degradation. Finally, the concentration of test compound was quantified by LC-MS. The percentage of test compound remaining (relative to the 0 min time point) at the individual time points is then reported. All experiments were performed in duplicate.

6.4. Human plasma stability

The plasma stability of compounds **13**, **15**, **16**, **17** and **31** was evaluated. Briefly, plasma is warmed to 37 °C for 10 min, mixed and centrifuged to pellet any aggregated protein. Plasma is equilibrated to 37 °C and biotransformation is initiated by addition of compound solution (2.5 μL, 10 μM final incubation concentration), and mixing. At each specified time-point (0, 15, 30, 60, 120 and 180 min), test compounds were removed into 200 μL ice-cold methanol to stop degradation. Internal standard was added during the quenching phase. Finally, the concentration of test compound was quantified by LC-MS. The percentage of test compound remaining (relative to the 0 min time point) at the individual time points is then reported. The *in-vitro* plasma half-lives ($t_{1/2}$) were calculated using the expression $t_{1/2} = 0.693/b$, where b is the slope found in the linear fit of the natural logarithm of the fraction remaining of the parent compound vs. incubation time.

[58]. All experiments were performed in duplicate. As controls were used, procaine (low stability) and procainamide (high stability).

6.5. In-vitro drug metabolism using human liver microsomes

For CYPs microsomal stability assay (CYP), 2.5 μL of sample (1 mM) with 100 mM phosphate buffer (pH 7.4) was incubated with 25 μL of 5 mg/mL human (CD-1) microsomes (Thermo Fisher Scientific, Bremen, Germany).

For CYPs and UGTs "dual-activity" microsomal stability assay (CYP-UGT), 25 μL of 5 mg/mL human were pre-incubated with alamethicin, which forms pores in microsomal membranes, promoting access of substrate and cofactor to UGT enzymes.

The reaction was initiated by adding 50 μL of mix NADPH 10 mM (CYP) or NADPH 10 mM and UDPGA 10 mM (CYP-UGT) as cofactors (1:1 v/v) and carried out 37 °C for 15, 30, 45, and 60 min in a Thermomixer comfort (Eppendorf, Hamburg, Germany).

The reaction was stopped by the addition of 200 μL ice-cold acetonitrile containing IS, and then samples were centrifuged at 14,000 rpm at 25 °C for 5 min (Eppendorf® microcentrifuge 5424, Hamburg, Germany). The supernatants were collected and injected in LC-MS.

The control at 0 min was obtained by addition of the organic solvent immediately after incubation with microsomes. As the positive controls were used testosterone (low stability in CYP activation), 2-naphthol (low stability CYP-UGT activation) and 3-(α-acetonylbenzyl)-4-hydroxy (high stability in dual activity assay). As the negative control was prepared by incubation up to 60 min without NADPH (CYP) or UDPGA/NADPH (CYP-UGT). The negative control is essential to detect problems such as non-specific protein binding or heat instability.

The natural logarithm of remaining concentration of parent compound was plotted vs. time (min). *In-vitro* intrinsic clearance was calculated as $CLint_{in\text{-}vitro} = (1000) \times (0.693/t_{1/2})/0.5$. The intrinsic *in-vitro* clearance was scaled to the intrinsic *in-vivo* clearance ($CLint_{in\text{-}vivo}$) using human physiology-based scaling factor (PBSF): $CLint_{in\text{-}vivo} = CLint_{in\text{-}vitro} \times$ PBSF (microsome protein/gram liver: 32 × gram liver/kg b. w.: 25.7) [59]. All experiments were performed in duplicate.

Funding

This work was supported by Ministero dell'Università e della Ricerca (MUR) project PIR01_00032 BIO OPEN LAB BOL "CUP" J37E19000050007, Project CIR01_00032-BOL"BIO OPEN LAB"-Rafforzamento del Capitale Umano and project "Pathogen Readiness Platform for CERIC ERIC upgrade" PRP@CERIC "CUP" J97G22000400006.

CRediT authorship contribution statement

Tania Ciaglia: Investigation. **Vincenzo Vestuto:** Investigation. **Veronica Di Sarno:** Methodology. **Simona Musella:** Methodology. **Gerardina Smaldone:** Investigation. **Francesca Di Matteo:** Investigation. **Valeria Napolitano:** Investigation. **Maria Rosaria Miranda:** Data curation, Formal analysis. **Giacomo Pepe:** Data curation, Formal analysis. **Manuela Giovanna Basilicata:** Investigation. **Sara Novi:** Validation. **Ilaria Capolupo:** Investigation. **Giuseppe Bifulco:** Writing – original draft, Writing – review & editing. **Pietro Campiglia:** Conceptualization, Funding acquisition. **Isabel Gomez-Monterrey:** Conceptualization, Writing – review & editing. **Robert Snoeck:** Investigation, Writing – original draft. **Graciela Andrei:** Conceptualization, Writing –

original draft. **Michele Manfra:** Data curation. **Carmine Ostacolo:** Conceptualization, Writing – original draft, Writing – review & editing. **Gianluigi Lauro:** Conceptualization, Investigation. **Alessia Bertamino:** Conceptualization, Data curation, Writing – original draft, Writing – review & editing.

Declaration of competing interest

The authors declare the following financial interests/personal relationships which may be considered as potential competing interests: Pietro Campiglia reports financial support was provided by Italian Ministry of University and Research. If there are other authors, they declare that they have no known competing financial interests or personal relationships that could have appeared to influence the work reported in this paper.

Data availability

Data will be made available on request.

Acknowledgments

The authors wish to express their gratitude to the Rega Institute collaborators Leentje Persoons and Brecht Dirix for excellent assistance in the cell-based assays.

Appendix A. Supplementary data

Supplementary data to this article can be found online at https://doi.org/10.1016/j.ejmech.2024.116128.

References

[1] https://covid19.who.int/, lastly. (Accessed 23 October 2023).
[2] H. Yang, Z. Rao, Structural biology of SARS-CoV-2 and implications for therapeutic development, Nat. Rev. Microbiol. 19 (2021) 685–700.
[3] L.D. Hayes, J. Ingram, N.F. Sculthorpe, More than 100 persistent symptoms of SARS-CoV-2 (long COVID): a scoping review, Front. Med. 8 (2021) 750378.
[4] C. Stasi, S. Fallani, F. Voller, C. Silvestri, Treatment for COVID-19: an overview, Eur. J. Pharmacol. 889 (2020) 173644.
[5] C. Wu, Y. Liu, Y. Yang, P. Zhang, W. Zhong, Y. Wang, Q. Wang, Y. Xu, M. Li, X. Li, M. Zheng, L. Chen, H. Li, Analysis of therapeutic targets for SARS-CoV-2 and discovery of potential drugs by computational methods, Acta Pharm. Sin. B 10 (2020) 766–788.
[6] N. Murakami, R. Hayden, T. Hills, H. Al-Samkari, J. Casey, L. Del Sorbo, P. R. Lawler, M.E. Sise, D.E. Leaf, Therapeutic advances in COVID-19, Nat. Rev. Nephrol. 19 (2023) 38–52.
[7] H.X.J. Lin, S. Cho, V. Meyyur Aravamudan, H.Y. Sanda, R. Palraj, J.S. Molton, I. Venkatachalam, Remdesivir in Coronavirus Disease 2019 (COVID-19) treatment: a review of evidence, Infection 49 (2021) 401–410.
[8] H. Li, M. Gao, H. You, P. Zhang, Y. Pan, N. Li, L. Qin, H. Wang, D. Li, Y. Li, H. Qiao, L. Gu, S. Xu, W. Guo, N. Wang, C. Liu, P. Gao, J. Niu, J. Cao, Y. Zheng, Association of nirmatrelvir/ritonavir treatment on upper respiratory severe acute respiratory syndrome coronavirus 2 reverse transcription-polymerase chain reaction (SARS-Cov-2 RT-PCR) negative conversion rates among high-risk patients with coronavirus disease 2019 (COVID-19), Clin. Infect. Dis. 76 (2023) e148–e154.
[9] E. Zarenezhad, M. Marzi, Review on molnupiravir as a promising oral drug for the treatment of COVID-19, Med. Chem. Res. 31 (2022) 232–243.
[10] Y.-C. Hwang, R.-M. Lu, S.-C. Su, P.-Y. Chiang, S.-H. Ko, F.-Y. Ke, K.-H. Liang, T.-Y. Hsieh, H.-C. Wu, Monoclonal antibodies for COVID-19 therapy and SARS-CoV-2 detection, J. Biomed. Sci. 29 (2022) 1.
[11] K. Widyasari, J. Kim, A Review of the currently available antibody therapy for the treatment of coronavirus disease 2019 (COVID-19), Antibodies 12 (2023) 5.
[12] F. Mazzaferri, M. Mirandola, A. Savoldi, P. De Nardo, M. Morra, M. Tebon, M. Armellini, G. De Luca, L. Calandrino, L. Sasset, D. D'Elia, E. Sozio, E. Danese, D. Gibellini, I. Monne, G. Scroccaro, N. Magrini, A. Cattelan, C. Tascini, E. Tacconelli, Exploratory data on the clinical efficacy of monoclonal antibodies against SARS-CoV-2 Omicron variant of concern, Elife 11 (2022) e79639.
[13] F. Ferron, L. Subissi, A.T. Silveira De Morais, N.T.T. Le, M. Sevajol, L. Gluais, E. Decroly, C. Vonrhein, G. Bricogne, B. Canard, I. Imbert, Structural and molecular basis of mismatch correction and ribavirin excision from coronavirus RNA, Proc. Natl. Acad. Sci. USA 115 (2017) E162–E171.
[14] M.R. Denison, R.L. Graham, E.F. Donaldson, L.D. Eckerle, R.S. Baric, Coronaviruses: an RNA proofreading machine regulates replication fidelity and diversity, RNA Biol. 8 (2011) 270–279.
[15] Y.M. Bar-On, A. Flamholz, R. Phillips, R. Milo, SARS-CoV-2 (COVID-19) by the numbers, Elife 9 (2020) e57309.
[16] http://who.int/activities/tracking-SARS-Cov-2-variants. (Accessed 23 October 2023) lastly accessed.
[17] S. Chatterjee, M. Bhattacharya, S. Nag, K. Dhama, C. Chakraborty, A detailed overview of SARS-CoV-2 omicron: its sub-variants, mutations and pathophysiology, clinical characteristics, immunological landscape, immune escape, and therapies, Viruses 15 (2023) 167.
[18] C.C. Giron, A. Laaksonen, F.L. Barroso da Silva, Differences between Omicron SARS-CoV-2 RBD and other variants in their ability to interact with cell receptors and monoclonal antibodies, J. Biomol. Struct. Dyn. 41 (2023) 5707–5727.
[19] W.-Y. Ching, P. Adhikari, B. Jawad, R. Podgornik, Effect of delta and omicron mutations on the RBD-SD1 domain of the spike protein in SARS-CoV-2 and the omicron mutations on RBD-ACE2 interface complex, Int. J. Mol. Sci. 23 (2022) 10091.
[20] M. Hoffmann, N. Krüger, S. Schulz, A. Cossmann, C. Rocha, A. Kempf, I. Nehlmeier, L. Graichen, A.-S. Moldenhauer, M.S. Winkler, M. Lier, A. Dopfer-Jablonka, H.-M. Jäck, G.M.N. Behrens, S. Pöhlmann, The omicron variant is highly resistant against antibody-mediated neutralization: implications for control of the COVID-19 pandemic, Cell 185 (2022) 447–456, e411.
[21] Y. Araf, F. Akter, Y.d. Tang, R. Fatemi, M.S.A. Parvez, C. Zheng, M.G. Hossain, Omicron variant of SARS-CoV-2: genomics, transmissibility, and responses to current COVID-19 vaccines, J. Med. Virol. 94 (2022) 1825–1832.
[22] E. Callaway, Omicron-specific vaccines protect as much as current jabs, Nature 609 (2022) 232–233.
[23] https://www.ema.europa.eu/en/news/adapted-vaccine-targeting-ba4-ba5-omicron-variants-original-sars-cov-2-recommended-approval. (Accessed 23 October 2023) lastly accessed.
[24] K. Steuten, H. Kim, J.C. Widen, B.M. Babin, O. Onguka, S. Lovell, O. Bolgi, B. Cerikan, C.J. Neufeldt, M. Cortese, R.K. Muir, J.M. Bennett, R. Geiss-Friedlander, C. Peters, R. Bartenschlager, M. Bogyo, Challenges for targeting SARS-CoV-2 proteases as a therapeutic strategy for COVID-19, ACS Infect. Dis. 7 (2021) 1457–1468.
[25] R. Banerjee, L. Perera, L.M.V. Tillekeratne, Potential SARS-CoV-2 main protease inhibitors, Drug Discov. Today 26 (2021) 804–816.
[26] Z. Lv, K.E. Cano, L. Jia, M. Drag, T.T. Huang, S.K. Olsen, Targeting SARS-CoV-2 proteases for COVID-19 antiviral development, Front. Chem. 9 (2022) 819165.
[27] S.G. Katre, A.J. Asnani, K. Pratyush, N.G. Sakharkar, A.G. Bhope, K.T. Sawarkar, V. S. Nimbekar, Review on development of potential inhibitors of SARS-CoV-2 main protease (MPro), Futur J. Pharm. Sci. 8 (2022) 36.
[28] S. Di Micco, R. Rahimova, M. Sala, M.C. Scala, G. Vivenzio, S. Musella, G. Andrei, K. Remans, L. Mammri, R. Snoeck, G. Bifulco, F. Di Matteo, V. Vestuto, P. Campiglia, J.A. Márquez, A. Fasano, Rational design of the zonulin inhibitor AT1001 derivatives as potential anti SARS-CoV-2, Eur. J. Med. Chem. 244 (2022) 114857.
[29] C.P. Gomes, D.E. Fernandes, F. Casimiro, G.F. da Mata, M.T. Passos, P. Varela, G. Mastroianni-Kirsztajn, J.B. Pesquero, Cathepsin L in COVID-19: from pharmacological evidences to genetics, Front. Cell. Infect. Microbiol. 10 (2020) 589505.
[30] M.-M. Zhao, W.-L. Yang, F.-Y. Yang, L. Zhang, W.-J. Huang, W. Hou, C.-F. Fan, R.-H. Jin, Y.-M. Feng, Y.-C. Wang, J.-K. Yang, Cathepsin L plays a key role in SARS-CoV-2 infection in humans and humanized mice and is a promising target for new drug development, Signal Transduct. Targeted Ther. 6 (2021) 134.
[31] A.S. Ashhurst, A.H. Tang, P. Fajtová, M.C. Yoon, A. Aggarwal, M.J. Bedding, A. Stoye, L. Beretta, D. Pwee, A. Drelich, D. Skinner, L. Li, T.D. Meek, J. H. McKerrow, V. Hook, C.-T. Tseng, M. Larance, S. Turville, W.H. Gerwick, A. J. O'Donoghue, R.J. Payne, Potent anti-SARS-CoV-2 activity by the natural product gallinamide A and analogues via inhibition of cathepsin L, J. Med. Chem. 65 (2021) 2956–2970.
[32] R. Milan Bonotto, A. Mitrović, I. Sosič, P. Martinez-Orellana, F. Dattola, S. Gobec, J. Kos, A. Marcello, Cathepsin inhibitors nitroxoline and its derivatives inhibit SARS-CoV-2 infection, Antivir. Res. 216 (2023) 105655.
[33] A. Madadlou, Food proteins are a potential resource for mining cathepsin L inhibitory drugs to combat SARS-CoV-2, Eur. J. Pharmacol. 885 (2020) 173499.
[34] M.D. Sacco, C. Ma, P. Lagarias, A. Gao, J.A. Townsend, X. Meng, P. Dube, X. Zhang, Y. Hu, N. Kitamura, B. Hurst, B. Tarbet, M.T. Marty, A. Kolocouris, Y. Xiang, Y. Chen, J. Wang, Structure and inhibition of the SARS-CoV-2 main protease reveal strategy for developing dual inhibitors against M(pro) and cathepsin L, Sci. Adv. 6 (2020) eabe0751.
[35] X.R. Ma, Y.R. Alugubelli, Y. Ma, E.C. Vatansever, D.A. Scott, Y. Qiao, G. Yu, S. Xu, W.R. Liu, MPI8 is potent against SARS-CoV-2 by inhibiting dually and selectively the SARS-CoV-2 main protease and the host cathepsin L, ChemMedChem 17 (2021) e202100456.
[36] E. Costanzi, M. Kuzikov, F. Esposito, S. Albani, N. Demitri, B. Giabbai, M. Camasta, E. Tramontano, G. Rossetti, A. Zaliani, P. Storici, Structural and biochemical analysis of the dual inhibition of MG-132 against SARS-CoV-2 main protease (Mpro/3CLpro) and human cathepsin-L, Int. J. Mol. Sci. 22 (2021) 11779.
[37] V. Di Sarno, G. Lauro, S. Musella, T. Ciaglia, V. Vestuto, M. Sala, M.C. Scala, G. Smaldone, F. Di Matteo, S. Novi, M.F. Tecce, O. Moltedo, G. Bifulco, P. Campiglia, I.M. Gomez-Monterrey, R. Snoeck, G. Andrei, C. Ostacolo, A. Bertamino, Identification of a dual acting SARS-CoV-2 proteases inhibitor through in silico design and step-by-step biological characterization, Eur. J. Med. Chem. 226 (2021) 113863.
[38] D. Dana, S.K. Pathak, A review of small molecule inhibitors and functional probes of human cathepsin L, Molecules 25 (2020) 698.

[39] S.R. Chowdhury, S. Kennedy, K. Zhu, R. Mishra, P. Chuong, A. Nguyen, S. G. Kathman, A.V. Statsyuk, Discovery of covalent enzyme inhibitors using virtual docking of covalent fragments, Bioorg. Med. Chem. Lett 29 (2019) 36–39.
[40] S.F. Chowdhury, L. Joseph, S. Kumar, R.T. Shenoy, S. Bhat, E. Ziomek, R. Ménard, J. Sivaraman, E.O. Purisima, Exploring inhibitor binding at the S′ subsites of cathepsin L, J. Med. Chem. 51 (2008) 1361–1368.
[41] A. Fujishima, Y. Imai, T. Nomura, Y. Fujisawa, Y. Yamamoto, T. Sugawara, The crystal structure of human cathepsin L complexed with E-64, FEBS Lett. 407 (1997) 47–50.
[42] G. La Monica, A. Bono, A. Lauria, A. Martorana, Targeting SARS-CoV-2 main protease for treatment of COVID-19: covalent inhibitors structure-activity relationship insights and evolution perspectives, J. Med. Chem. 65 (2022) 12500–12534.
[43] Y. Li, K. Wang, H. Sun, S. Wu, H. Wang, Y. Shi, X. Li, H. Yan, G. Yang, M. Wu, Y. Li, X. Ding, S. Si, J. Jiang, Y. Du, Y. Li, B. Hong, Omicsynin B4 potently blocks coronavirus infection by inhibiting host proteases cathepsin L and TMPRSS2, Antivir. Res. 214 (2023) 105606.
[44] M. Parmar, R. Thumar, B. Patel, M. Athar, P.C. Jha, D. Patel, Structural differences in 3C-like protease (Mpro) from SARS-CoV and SARS-CoV-2: molecular insights revealed by molecular dynamics simulations, Struct. Chem. 34 (2022) 1309–1326.
[45] K.S. Pang, Y.R. Han, K. Noh, P.I. Lee, M. Rowland, Hepatic clearance concepts and misconceptions: why the well-stirred model is still used even though it is not physiologic reality? Biochem. Pharmacol. 169 (2019) 113596.
[46] C.A. McNaney, D.M. Drexler, S.Y. Hnatyshyn, T.A. Zvyaga, J.O. Knipe, J. V. Belcastro, M. Sanders, An automated liquid chromatography-mass spectrometry process to determine metabolic stability half-life and intrinsic clearance of drug candidates by substrate depletion, Assay Drug Dev. Technol. 6 (2008) 121–129.
[47] H. Lu, Stereoselectivity in drug metabolism, Expet Opin. Drug Metabol. Toxicol. 3 (2007) 149–158.
[48] Z. Shen, C. Lv, S. Zeng, Significance and challenges of stereoselectivity assessing methods in drug metabolism, J. Pharm. Anal. 6 (2016) 1–10.
[49] J. Shaman, M. Galanti, Will SARS-CoV-2 become endemic? Science 370 (2020) 527–529.
[50] A. Katzourakis, COVID-19: endemic doesn't mean harmless, Nature 601 (2022) 485.
[51] D.X. Liu, J.Q. Liang, T.S. Fung, Human coronavirus-229e, -OC43, -NL63, and -HKU1 (Coronaviridae), in: D.H. Bamford, M. Zuckerman (Eds.), Encyclopedia of Virology, fourth ed., Academic press, Cambridge, 2021, pp. 428–440.
[52] L.A. Hardegger, B. Kuhn, B. Spinnler, L. Anselm, R. Ecabert, M. Stihle, B. Gsell, R. Thoma, J. Diez, J. Benz, J.M. Plancher, G. Hartmann, D.W. Banner, W. Haap, F. Diederich, Systematic investigation of halogen bonding in protein–ligand interactions, Angew. Chem. Int. Ed. 50 (2010) 314–318.
[53] W. Dai, B. Zhang, X.-M. Jiang, H. Su, J. Li, Y. Zhao, X. Xie, Z. Jin, J. Peng, F. Liu, C. Li, Y. Li, F. Bai, H. Wang, X. Cheng, X. Cen, S. Hu, X. Yang, J. Wang, X. Liu, G. Xiao, H. Jiang, Z. Rao, L.-K. Zhang, Y. Xu, H. Yang, H. Liu, Structure-based design of antiviral drug candidates targeting the SARS-CoV-2 main protease, Science 368 (2020) 1331–1335.
[54] Schrödinger Release 2022-3: Protein Preparation Wizard; Epik - Impact - Prime, Schoredinger LLC, New York, 2023.
[55] Schrödinger Release 2022-3, LigPrep, Schrödinger, LLC, New York, NY, 2022.
[56] Schrödinger Release 2022-3: Glide, Schrödinger, LLC, New York, NY, 2022.
[57] L. Ozorio, C. Mellinger-Silva, L.M.C. Cabral, J. Jardin, G. Boudry, D. Dupont, The influence of peptidases in intestinal brush border membranes on the absorption of oligopeptides from whey protein hydrolysate: an ex vivo study using an Ussing chamber, Foods 9 (2020) 1415.
[58] R. Konsoula, M. Jung, In vitro plasma stability, permeability and solubility of mercaptoacetamide histone deacetylase inhibitors, Int. J. Pharm. 361 (2008) 19–25.
[59] Y. Chen, F. Zhu, J. Hammill, G. Holbrook, L. Yang, B. Freeman, K.L. White, D. M. Shackleford, K.G. O'Loughlin, S.A. Charman, J.C. Mirsalis, R.K. Guy, Selecting an anti-malarial clinical candidate from two potent dihydroisoquinolones, Malar. J. 20 (2021) 107.